Discharge Characteristics of V-Shaped Multi-Slit Weirs

Kai Ji

A thesis

In the Department of

Building, Civil and Environmental Engineering

Presented in Partial Fulfillment of the Requirements

For the Degree of Master of Applied Science in Civil Engineering at

Concordia University

Montreal, Quebec, Canada

March 2007

Your file Votre référence
ISBN: 978-0-494-28901-3
Our file Notre référence
ISBN: 978-0-494-28901-3

ABSTRACT

Discharge Characteristics of V-Shaped Multi-slit Weirs

Kai Ji

V-shaped weirs with small angles are efficient in accurately measuring extremely small discharge rates. The concept of slit weirs to measure discharge rates has been studied in recent investigations. Rectangular multi-slit notches or weirs have been shown to extend the range of flow measurement to include both very low and high discharge rates.

It is a well-known fact that V-notches whose sections are narrower at lower heads are preferred to rectangular notches to measure small discharge rates in laboratories. To increase the range of discharges measured, the concept of multi-slit weirs using rectangular weirs has been introduced recently. For rectangular multi-slit weirs, experimental data showed that the discharge coefficient C_d for multi-slit weirs or a single weir was a function of the Reynolds number R_e when R_e is based on the width of rectangular weirs.

V-notches are generally used for laboratory flow measurements, as they can very precisely measure discharge rates. Hence, the multi-slit weirs formed by V-notches are expected to measure discharges in a very wide range of discharge rates.

To represent a common discharge coefficient C_d for multi-slit weirs formed of either rectangular or triangular shaped individual weirs, a new Reynolds number R_{eR} is proposed to unify representation of discharge coefficient data for both rectangular shaped and V-

shaped multi-slit weir units. C_d data for both rectangular and V-shaped multi-slit weirs fall on a single curve and appear to be the function of R_{eR}. At large Reynolds number, R_{eR}, the discharge coefficient C_d approaches a constant value of 0.61. This constant also denotes the contraction coefficient for the narrow two-dimensional slit flow. Present test data show that C_d for multi-slit V- shaped weirs is generally a function of R_{eR} for $b/B<0.3$. Here, R_{eR} is based on the hydraulic radius R and b is the value of top flow width of the water passing the multi-slit weirs.

A very limited number of numerical simulations are also performed to determine discharge coefficient (C_d) and the water surface profiles for the multi-slit V-shaped weirs. The predictions related to the surface profile based on the numerical model are validated by experimental data. The three-dimensional (3D) two-equation standard $k-\varepsilon$ turbulence model together with the volume of fluid VOF tracking technique is effectively used to obtain a few simulation results that are limited in scope.

ACKNOWLEDGMENTS

I would like to thank Dr. Ramamurthy for suggesting the research topic on V-shaped multi-slit weirs. Additional thanks are due to Dr. Junying Qu and Mrs. Xiaoyang Che who have assisted me a great deal in the period of the study.

I would also like to express my appreciation to Mr. N. Lang for his help in the laboratory work. Finally, I express my thanks to my parents and wife, who give me great support.

Table of Content

Appendix

Three Dimensional Simulation of Flow Over V-Shaped Weirs (or Notches)

List of Notation

Notation

A = Cross sectional area;

b = Weir width;

B = Channel width;

c = Void fraction;

C_d = Discharge coefficient;

g = Gravitation acceleration;

h = Weir head;

k = Turbulent kinetic energy;

n = Slit number;

p = Weir height;

P = Wetted perimeter of the cross-section;

Q = Weir discharge;

Q_i = Discharge for the individual slit weir;

R_e = Reynolds number;

R_{eR} = Reynolds number based on hydraulic radius;

R = Hydraulic Radius;

S_{ij} =Strain-rate tensor;

u = Axial velocity (parallel to the horizontal conduit wall);

u_j = Average flow velocity (j = 1, 2 in two dimension, or j = 1, 2, 3 in three dimensions);

u_τ = Resultant friction velocity;

U_i or V_i = Average flow velocity;

We = Weber number;

x_i = Cartesian coordinate (i=1, 2 in two dimension, or i=1, 2, 3 in three dimensions);

X, Y and Z = Coordinates at three dimensions;

y = Normal distance to the wall;

y_c = Critical depth;

γ = Specific weight;

ρ = Water density;

μ = Dynamics viscosity;

σ = Surface tension;

ω = Specific dissipation rate;

ε = Dissipation rate;

τ_{ij} =stress rensor;

ν = Kinematic viscosity;

ν_T =eddy viscosity.

Common Abbreviations

3D - Three-dimensional;

CDS - Central difference scheme;

CFD - Computational fluid dynamics;

CV - Control volume;

DCS - Deferred correction scheme;

FVM - Finite volume method;

PISO - Pressure implicit splitting of operator;

PLS - Partial least squares;

QUICK - Quadratic upwind interpolation for convective kinematics;

RANS - Reynolds averaged Navier-Stokes;

SIMPLE - Semi-implicit method for pressure-linked equation;

UDS - Upwind difference scheme;

VOF - Volume of fluid;

List of Figures

List of Tables

Chapter 1

Introduction

1.1 General Remarks

The measurement of discharge belongs to a fundamental work in a system for water resources application and management. In engineering practice, some of the hydraulic structures encountered are used for distribution or concentration of water, and regulation of flows. Weirs and notches are hydraulic structures that are efficient measurement devices for water flow. They have been widely used and successfully investigated for a long time. It is noted that the triangle weirs, involving the V-notches, are more precise and have a larger range for discharge rate measurement.

The investigation of the flow characteristics of triangle weirs with large angles (>20°) have been conducted in the past. The present study is related to an experimental investigation to predict the characteristics of V-shaped multi-slit weirs. The behaviors of both the single and multi-slit units are presented.

In natural streams, where it is necessary to measure a wide range of discharge, a triangular control section has the advantage of providing a wide opening at high flows so that it causes no excessive backwater effects, whereas at low flows its opening is reduced so that the sensitivity of the measuring device remains acceptable.

It is easy to understand that the characteristics of the flow, such as flow patterns, velocity

distribution, pressure distribution and free surface profile are very important for engineering planning, design and operation as well as for measurement of flows. In practice, flows are turbulent, highly unsteady and three-dimensional. Weir flow characteristics can be obtained using experimental, analytical or numerical approaches. Both approaches have been used in the past. Due to present advanced computing techniques, most hydraulic problems can be solved numerically using commercial codes. However, the results are to be validated using test data.

Turbulence modeling in which Navier—Stokes equations are parts of the governing equations are frequently used to solve hydraulic problems. Computational Fluid Dynamic (CFD) with its general procedure can be used to describe the flow characteristics. The present study attempts to adopt this approach in a limited way for illustrating the flow pattern over the V-shaped multi-slit weir units by considering a few selected cases. The main aim however is to get the weir flow behavior based mainly on experimental data.

1.2 Literature Review

1.2.1 The free over fall flow

The free overfall (Fig. 1.1) can be viewed as a weir whose sill height is zero. There exists a unique relationship between the flow depth Ye, at the brink or the end section forming a free over fall and the flow rate, Q, in a rectangular open channel. The free over fall is the simplest measuring device. The term end depth ratio (EDR) denotes the ratio of the end depth, Ye, at the brink section to the critical depth, Yc, in the open channel. The free

over fall in a rectangular channel has been extensively studied by many investigators.

The free overfall in a rectangular channel has been extensively studied by Rouse (1936), Shaarawi (1954), Delleur (1956), Rajanatnam and Muralidhar(1968), Rajaratnam.et.al (1976), Bauer and Graf (1971), Ali and Sykes (1972), and Terzidis (1985). The EDR in circular and triangular channels has also been studied by Diskin (1961), Rajaratnam and Muralidhar (1964a, b), and Aliand Sykes (1972).

Hager (1983) applied the extended energy and momentum equations to the flow near an over fall and derived an expression relating EDR and the upstream Froude number. He also presented an expression for the surface profile near the brink section in a rectangular channel.

Studies on the free over fall in a trapezoidal channel are relatively few. Diskin (1961) performed the earliest theoretical and experimental investigation. Very good discussions of his work have been presented by Rajaratnam (1962), Hamid (1962) and Replogle (1962).

Keller and Fong (1993) studied the trapezoidal free over fall experimentally and theoretically considering the trapezoidal section as a combination of a rectangular and a triangular section involving a nonzero pressure distribution at the brink. Based on measurements of Replogle (1962), they derived a sixth-degree equation linking Ye (end depth) to Yc (critical depth), which requires an iterative numerical solution. Terzidis and

Anastasiadou-Partheniou (1990) studied the flow at the end section of a trapezoidal section using the test data of Replogle (1962) and Rajaratnam and Muralidhar. Their procedure is very practical to use. Base on published experimental data, Gupta et al (1993) presented a calibration curve for the prediction of discharge in a trapezoidal channel based on the end (brink) depth. Litsa Anastasiadou-Partheniou and Evangelos Hazigiannakis (1995) accounted for the convergence of streamlines while arriving at the relationship between EDR and the Froude number in the upstream channel.

1.2.2 Sharp-crested weir and notch flows

Sharp crested weirs are relatively precise and simple devices for open channel flow measurement. There are many types of sharp crested weirs in use, but the most common are rectangular weirs, suppressed rectangular weirs, triangular (V-notch) weirs, and trapezoidal (Cipolletti) weirs. All of these weirs have a number of features in common: the weir crest is a sharp plate, the flow jet over the crest must be fully aerated, and the discharge is proportional to the upstream head on the weir.[Bos. 1989]

Many discharge equations for different types of weirs have been developed in laboratory experiments. Schoder (1929) published the results of over 2,000 discharge measurements for 1,512 different heads on rectangular suppressed weirs of different heights and with different velocity profiles. These experiments were performed at Cornell University between 1904 and 1920 and utilized an open channel with a number of weir arrangements. Although weirs of various crest heights were tested, all of the weirs extended the full width of the channel (rectangular suppressed weirs). Velocities were measured in the

upstream channel, and baffles and stilling rafts were used to produce different velocity profiles. Discharge volumes were measured in a weighing tank at the end of the open channel and weir apparatus.

The experimenters arrived at a number of conclusions based on the weir measurements. The Francis formula was found acceptably accurate for weirs with sharp, square edges, a smooth vertical upstream face, a deep upstream pool behind the weir, and negligible effects of approach velocity.

It is widely understood that weir discharge equations are accurate to within about two percent as long as the head on the weir is carefully measured: caution should be used when assuming this range of accuracy. The head may be measured carefully, but there are a number of other conditions which may affect discharge by several percent. Slight roundness of the upstream weir edge results in the weir discharge increasing by several percent. Roughness of the weir plate near the crest was also found to increase the discharge even when the crest was sharp. Velocity distribution was also found to influence the weir discharge. It was concluded that if standard weir discharge equations are to be used, careful consideration should be given to measurement of the head on the weir but also to velocities in the upstream channel, weir sharpness, and general conditions of the weir plate. [Schoder, 1929]

In all cases, the weirs used for flow measurement should be built to standard conditions, and the upstream channel should be straight and uniform for a distance of at least ten

times the channel width so that no irregular flow conditions will be present at the weir. Some of the standard conditions given for small measurement weirs are described by Kraatz and Mahajan (1975). The weir crest should have a square upstream edge with a top thickness of between 1 and 2 mm. The downstream face of the weir should have a chamfer of at least 45° so that the water jet springs clear of the weir. For contracted weirs, the crest height should be greater than twice the depth of the maximum head on the weir, and the sides of the weir opening should be at least at a distance of twice the head from the side walls of the channel. Conditions other than these could affect the shape of the nappe (the water jet over the weir) and alter the weir discharge. The driving head on the weir (h) should meet the following criteria: $6\ cm \leq h \leq 60\ cm$, and the head on trapezoidal and rectangular weirs should be less than or equal to one third of the crest length. Very low heads should be avoided because the jet will cling to the weir face rather than springing clear. The weir crest must be level and straight. The weir crest must be higher than the downstream water surface so that the weir can discharge freely. Sharp crested weirs are not intended to operate under submerged flow conditions.

A free fall of the nappe is required for sharp crested weirs to operate properly, and this requires some fall in the channel. Sharp crested weirs may not be practical to use in channels with very flat slopes because the backwater curve created behind the weir may extend for miles and require expensive raising of the channel banks to contain the water. The bottom of the channel directly downstream of the weir crest is subjected to high pressures due to the impact of the falling nappe, and channel protection is required in this area (Papoutsi-Psychoudaki, 1988). Due to the extensive channel protection that would

be required for weirs with high heads and large flow rates, sharp crested weirs are generally limited to relatively small-scale applications (the Bureau of Reclamation, 1974 gives a maximum flowrate in their sharp crested weir discharge tables of about 100 cfs).

A large number of studies have been devoted to the problem of rectangular sharp-crested weirs in the past (Bos, 1989). Kindsvater and Carter (1957) presented a comprehensive solution for the weir discharge characteristics based on test data and dimensional analysis. Based on their experimental results, Kandaswamy and Rouse (1957) identified two distinct ranges for the flow over a rectangular sharp-crested weir in terms of the weir parameter *h/p*. Here, h denotes the driving head and p denotes the height of the weir bottom (Fig 2.3). The *h/p* ratio is a measure of the affect of the approach velocity head. It is also complementary to *b/B* as an area-contraction ratio. Its influence is said to be represented by a velocity-of-approach term in several published formulas. Actually, for the boundary conditions specified, the flow in the approach channel is always sub-critical, and flow with minimum specific energy always occurs in the vicinity of the weir crest. Ramamurthy (1987) et.al and Rajaratnam and Muralidhar (1971) used experimental data related to velocity and pressure distribution to predict a relationship between the discharge coefficient, C_d, and h/p for rectangular sharp-crested weirs.

Bos. (1989) noted that the effective discharge coefficient (C_e) in the basic equation for a V-shaped (sharp crested) notch or weir is a function of three main variables:

$$Ce = f[\frac{h}{p}, \frac{p}{B}, \theta] \tag{1-1}$$

Where,

p = height of V-shaped weir crest;

B=width of channel;

θ = the angle of V-shaped weir, $(20° < \theta < 120°)$;

h = head over the crest weirs.

It is obvious that Eq. (1-1) did not consider directly the influence of the flow regime over the V-shaped (sharp-crested) weir. Bos. (1989) recommended a flow rating table for θ = 90°, 45°and 22.5° V-shaped sharp-crest weirs.

In engineering practice, the use of sharp crested weirs is limited by several constraints. Because weirs trap sediments very effectively, weirs should be used only where the flow is relatively free of sediments and debris. Weirs used in flows carrying sediment should have gates in the bottom that can be opened to flush the sediments from behind the weir, or other methods for periodic sediment removal should be provided to insure that the sediment does not accumulate excessively behind the weir. Before 1985, very little information about the use of these combined devices for flow measurements was available. Ahmed (1985) published his study on a combination of rectangular weir above a rectangular sluice without contraction. He tried to obtain a common discharge coefficient for the combined system, but his data were not enough to make generalization. Recently, this subject has attracted the researchers who tried to investigate experimentally the discharge characteristics of combined weirs and gates. Negm (1994) discussed the

effect of flow and geometric parameters on discharge characteristics of free flow through a combined rectangular contracted weir and a triangular gate of inverted V shape with angles ranging from 45 to 110 degree.

1.2.3 The slit weir flow

The slit weir is a very narrow rectangular sharp edged device at the end of an open channel capable of measuring low flow rates. Aydin (2002) stated that the discharge coefficient, C_d, over the slit weir is a function of Reynolds number, R_e, in the range of covered by his tests. According to Aydin (2002), C_d of rectangular slit weir can be express as follows:

$$C_d = 0.562 + (11.35 / R_{eb}^{0.5}) \tag{1-2}$$

Here, the Reynolds number R_e based on $L=b$, b denotes width of notch unit. And the Reynolds number could be calculated as:

$$R_{eb} = \frac{Q}{h\nu} \tag{1-3}$$

C_d = discharge coefficient ;

Q = flow rate;

h = head over the crest weir;

ν =kinematic viscosity.

Based on the hydrodynamic concept of images, Ramamurthy, et al (2005) suggested the use of a bank of multi-slit rectangular weirs to determine experimentally the discharge

coefficient by means of the measured discharges and the corresponding heads causing flow through multi-slit weirs. They concluded that the discharge coefficient can be represented solely as a function of the Reynolds number. These results have been extended to V-shaped multi- slit notches for flow measurement in the present study.

As mentioned above, the sharp-crested weir in a rectangular open channel can be taken as an effective device for flow measurement and control. Recently, the flow characteristics of the rectangular weirs were obtained by numerical modeling (Khan and Steffler 1996). They predicted the water surface profiles for sharp-crested weirs with sloping upstream faces, using a two-dimensional numerical model involving vertically averaged continuity, longitudinal momentum and vertical momentum equations. Wu and Rajaratnam (1996) experimentally determined the flow reduction factor for flow over sharp-crested weirs considering flow submersion. Martinez et al. (2005) presented the characteristics of compound sharp-crested weirs.

A separation zone occupied by a large eddy occurs in the corner between the weir plate and the bottom of the approach channel. The effect of this occurrence on a low weir, in comparison with the flow pattern for the same weir, is similar to the effect of having a sloping plate upstream of the weir. The comparable effect on discharge is the same as an increase in head. A separation zone also occurs in the corner between the side of a slit weir plate and the walls of the approach channel. The effect of this occurrence, in comparison with potential motion, is to reduce the width contraction of the weir nappe. Its influence on the discharge is the same as an increase in the width of the weirs.

However, no separation zone occurs between the slit weirs.

Viscous shear causes the flow to be retarded in the vicinity of the boundaries. This condition can be described with respect to potential motion by means of the discharge-displacement, boundary-layer thickness. On the surface of the weir plate, near the vertical edges of the notch as well as the horizontal crest, the effect of the boundary layer is similar to the effect of rounding the upstream corners of the notch. Compared with potential flow through a sharp-edged notch, therefore, the coefficient of contraction for the real fluid motion is larger. The effect on the discharge, in the other hand, is similar to the effect of increasing both h and b.

A boundary layer is also formed on the bottom and side walls of the approach channel. The effect of this occurrence on the discharge is similar to the effect of a reduction in the width of the width of the weir (b). For values of b/B less than 1.0 the effect of the side-wall boundary layers is to increase the effective value of b/B by decreasing the effective channel width (B). Similarly, the influence of the boundary layer on the bottom of the approach channel resembles the influence of a decrease in p. The effect of this occurrence on the discharge function, therefore, is similar to the effect of an increase in h/p.

Generally speaking, the relative effects of viscosity diminish as the size of the weir and the head on the weir increase.

1.3 Objectives of Present Study

The present study is mainly experimental and the analysis related to the interpretation of test data collected. The first part of the study mainly deals with V-shaped multi-slit weirs for measuring flow at both high and low discharge rates. The following objectives are covered in this section:

1) Develop an experimental set up to determine the flow characteristics of V-shaped multi-slit weirs (or notches) to measure a wide range of discharge rates.
2) Validate the concept of treating V-shaped (sharp-crested) slit weirs on either side of the central present weir of multi-slit weir unit as image weirs of the parent weir (Fig. 2.5a.b).
3) Determine the flow surface (central line) profile and obtain the parameters that determine the flow characteristics of the V-shaped multi-slit weir units.
4) Determine the universal dimensionless parameter that relates the discharge coefficients of both rectangular and V-shaped multi-slit units based on experimental data.

The second part of the study is limited in scope and deals very briefly with the application of a simple computational fluid dynamics (CFD) model to predict the flow behavior of the V-shaped multi-slit unit and validate the model predictions using the present test data. Only a few selected weir flows are considered in this section.

1.4 Thesis Configuration

A comprehensive solution is proposed for describing the discharge characteristics of both rectangular and V-shaped slit weir units. The solution is based on a simple relation connecting the weir discharge coefficient with the dimensionless parameter denoted as the Reynolds number based on the hydraulic radius R ($=A/P$). Here, A denotes the area and P denotes the wetted perimeter of the flow at the weir section.

Experimental data indicates that the fluid property such as surface tension is significant only in the low range of the driving head h ($h<$ 15cm) for narrow V-shaped weirs. The weir parameters such as the ratio nb/B denoting the dimensionless weir width are chosen to be very small so that it does not influence the discharge coefficient. Here, B denoted the channel width and b denotes the top width of the flow at the weir section. Further, the height p of the weir unit (Fig. 2.7) is expressed as a dimensionless parameter h/p. For the range of parameters covered in the present tests, it is shown that this parameter does not influence the weir unit's discharge coefficient significantly.

A short section also deals with the numerical simulation of the weir unit flow. The 3-dimensional k-ε model was selected for the turbulence modeling. The predicted weir flow characteristics are validated using test data. Values of the discharge coefficients were determined covering a wide range of the significant hydrodynamic and geometric parameters. Additional data to confirm the use of the proposed universal Reynolds number that represented both rectangular and V-shaped multi-slit units well have

obtained from published experimental results of other investigators.

This thesis consists of five chapters and one appendix. The first chapter provides an introduction to the proposed study and the existing literature. It also states the scope of the study. Chapter 2 deals with the hydraulic principles and basic features of the single and V-shaped multi-slit (sharp-crested) weirs used for discharge rate measurements. Chapter 3 covers the experimental set-up, procedures and data analysis as well as presentation of results. In Chapter 4, the analysis and discussion of the results are made using both the present and existing data. This chapter is inclusive of the variation of C_d with the generalized Reynolds number R_e and W_e as well as *b/B, h/p*. Chapter 5 deals with the summary, conclusions and the scope for future study. Appendix very briefly introduces the three dimensional (3D) turbulence model including boundary conditions, algorithm and the application of CFD code for open channel flows.

Chapter 2

Flow Over V-Shaped Multi-Slit (Sharp-Crested) Weir

This chapter introduces the hydraulic principles and basic features of single V-shaped slit (sharp-crested) weir and the V-shaped multi-slit (sharp-crested) weir units in a rectangular open channel used for discharge rate measurements.

2.1 Hydraulic Principles

According to hydraulic principles, for accelerating flow in a rectangular open channel which is straight and very short, the loss of energy head is negligible. Two basic equations are applicable (Fig 2.1).

Continuity equation:

$$Q = \overline{V}_1 A_1 = \overline{V_2} A_2 \tag{2-1}$$

Here, Q is discharge; $\overline{V_1}$, $\overline{V_2}$ are average velocities at cross sections 1 and 2; A_1, A_2 are the areas of the two cross-sections.

Bernoulli's equation:

$$H = \alpha_1 \frac{\overline{V_1^2}}{2g} + [Y_1 + Z_1] = \alpha_2 \frac{\overline{V_2^2}}{2g} + [Y_2 + Z_2] \tag{2-2}$$

Here, H is the total energy head, $\alpha_1 \frac{\overline{V_1^2}}{2g}, \alpha_2 \frac{\overline{V_2^2}}{2g}$ are velocity heads at the two cross-sections consider, Y_1 and Y_2 are the flow depths and Z_1 and Z_2 are the elevation heads. Also, α_1 and α_2 are the velocity coefficients accounting for nonuniform velocity distribution (Chow 1959).

In Eq. (2-1) and (2-2) the piezometer levels, $[Y_1 + Z_1]$ and $[Y_2 + Z_2]$ denote the water surface levels. Knowing the shapes of the two cross-sections, A_1 and A_2 can be obtained. Using these data, the velocities $\overline{V}_1$ and $\overline{V}_2$ can be determined.

Under critical flow condition, the specific energy is the minimum. For a given discharge rate, the water level and the discharge rate should present a unique relationship in the short zone i.e., there is only one value for the critical depth of flow. Also, there exists the following equation for critical flow:

$$\alpha \frac{\overline{V_c}^2}{2g} = \frac{A_c}{2B_c} \tag{2-3}$$

Here,

α = velocity distribution coefficient, commonly being unity ;

c= subscript denoting critical condition;

A=area of cross-section;

B=width of cross-section.

It is noted that Eq. (2-3) is valid for steady flow with parallel streamline in a small slope channel only.

From Eq. (2-3), the $\overline{V}$ at critical flow can be obtained:

$$\overline{V} = \overline{V_c} = (g \frac{A_c}{B_c})^{1/2} \tag{2-4}$$

In other words, the criterion for critical flow (critical velocity) can be obtained. Knowing the end depth at the brink section one can obtain the discharge rate Q for the open channel flow. The end depth is a function of the channel slope. The over fall flow is sometimes considered as flow through a weir whose height $H = 0$. There are several types of critical flow meters. For instance, the Parshall flume commonly used in the United States is a critical flow meter. It is a self-cleansing flume. However, these flumes are not geometrically similar (Chow 1959).

2.2 Basic Feature

The V-shaped (sharp-crested) or thin-plate weir is an overflow structure whose crest length in the direction of flow is equal to or less than 2mm, and the weir plate should be smooth and plane, especially on the upstream face so that even at a minimum head the nappe is completely free from the weir body after passing the weir and no adhering nappe can occur (Bos, 1989) (see Fig 2.2 and Fig 2.3).

According to Bos. (1989), based on the limitations of the $\frac{h}{p}, \frac{h}{B}, h, p$ and B, the V-shaped (sharp-crested) weirs may be classified into two types: partially contracted and fully contracted, which would result in different flow regimes. But from a hydraulic point of view, the weir may be fully contracted at low heads while at increasing h values it becomes partially contracted.

Fig.2.3 shows that to some extent, the concept of critical flow is not applicable for a sharp-crested weir. The following assumptions are made for the derivation of the weir

discharge equations. The sharp-crested weir can be viewed as an orifice with a free water surface; the height of water level above the weir crest is $h = h_1$; there is no contraction, flow velocity over the weir crest tends to be horizontal. Also, the approach velocity head $\frac{V_1^2}{2g}$ can be neglected. Then, the formula for calculating the velocity at an arbitrary point of the control section was derived, (Bos.1989)

$$V' = \sqrt{2g(h_1 + V_1^2/2g - m)} \tag{2-5}$$

and the discharge rate over the V-shaped weir can be taken:

$$Q = (2g)^{0.5} \int_0^{h_1} x(h_1 - m)^{0.5} dm \tag{2-6}$$

Here, the total flow over the weir can be obtained by integration between m=0-h_1; variable x denotes the width of free water surface on the top of V-notch, and it is a function of m (Fig. 2.3).

To get the exact discharge rate Q, one can use an effective discharge coefficient C_d to adjust Eq. (2-6),

$$Q = C_d (2g)^{0.5} \int_0^{h_1} x(h - m)^{0.5} dm \tag{2-7}$$

At the control section of the V-shaped (sharp-crested) weir, Eq.(2-7) can be written as follows:

$$Q = C_d (2g)^{0.5} \int_0^h \left[2 \tan \frac{\theta}{2} \right] m(h-m)^{0.5} \, dm \tag{2-8}$$

i.e.,

$$Q = C_d \frac{8}{15} (2g)^{0.5} \tan \frac{\theta}{2} h^{2.5} \tag{2-9}$$

Here,

$x = 2m \tan \frac{\theta}{2}$, $h_1 = h$, and θ denotes angle of the V-notch.

Thereafter, the Eq. (2-9) is used as the basic equation in present study.

The traditional form of the basic equation of discharge is obtained by integrating an approximate velocity Eq. (2-5) and an approximate area. This basic equation must be modified by a combination of dimensional analysis and experiment data. Thus, based on the piezometric head, h, if the reference level is known, C_d is the key for determining the relationship between the discharge rate Q, and head h_1. But the value of C_d is affected by a number of factors obtained by experiment.

Kindsvater and Cater (1957) made some modifications for applying Eq. (2-8) to both fully and partially contracted V-shaped (sharp-crest) weir with $h_e = h + k_n$. They called h_e as the effective head. Here, k_n not only represents the combined effects of the fluid properties, but is also empirically a function of the angle θ. It means that the C_d is a function of following variables:

$$C_d = f\left[\frac{h_1}{p_1}, \frac{p_1}{B_1}, \theta\right] \tag{2-10}$$

where the subscript denotes in the measure section.

The present study explores the effects of the flow properties of weirs on C_d by using experiments and analysis. Firstly, the Reynolds number R_e, and the Weber number W_e represent the influence of the viscosity and surface tension of water respectively. Secondly, the shapes and the notch angle θ represent the geometric factors of weirs in open channels. Thirdly, the flow characteristics of single slit and multislit V-shaped sharp-crested weirs are explicated by the combined effects of the different factors.

2.3 Multi-slit Sharp-Crested V-notch

The slit V-notch is one of the most precise discharge rate measuring devices for flow rates. To permit the slit weir to measure a wide range of flow rates, one can use a bank of identical slit weirs in which each weir is an image of the neighboring weir. It may be permitted to interpret the dividing streamline between two adjacent weirs as a solid boundary (Fig. 2.5). In the present study, this concept is used to predict the flow characteristics of multislit weirs, which consist of 7 slit V-shaped (sharp-crested) weirs, Fig. 2.6 is capable of measuring a wide range of flow rates. This is achieved by blocking appropriate weirs to suit system of N multi-slit weirs in which n weirs are active (not blocked), the effective weir width ratio is *(nb)/B*.

In the present tests, *(nb)/B* is varied from 0.005 to 0.187. Consequently, for these *(nb)/B*

values, the corresponding theoretical contraction coefficient for flow past a two-dimension slit is close to 0.61[Olson 1980]. The range of dimension parameters chosen for tests is shown in Table 2.1.

For the slit weirs A1, B1 and C1 (Fig. 2.5a) of the multi-slit weir unit (n=3) set in the channel of width B, the streamlines EF, GH, IJ and KL are also the stagnation streamlines. As such, the streamlines GH and IJ can be replaced by solid boundaries.

Consequently, the slit weirs A1 and C1 can be considered to be images of the parent slit weir B1. Theoretically the three weirs A1, B1 and C1 can be viewed as identical single weirs whose effective width ratio is *3b/B*. This procedure was adopted while analyzing the 3 multi-slit weir units. The error in the direct measurement of flow rates through single slit weir of multi-slit weir units is shown in Table 2.2. It shows that the previous concept of images is applicable for extending the range of discharge measurement using multi-slit weirs. However in practice, the slightly non-uniform distribution of the approach velocity in the main channel will result in small difference in the flow through the individual multi-slit weirs.

Based on the knowledge as mentioned above, the experimental device was developed to validate the image weir concept and get test data to analyze the relationship between discharge coefficient and characteristics of weir flow which will describe in the next chapter.

Chapter 3

Experimental Set-up and Procedures

This chapter deals with the details of the experimental set-up and procedures.

3.1 Experimental Set-up

Experiments were conducted in a rectangular, horizontal, mild steel flume 60 cm wide and 1085 cm long (Fig. 3.1), whose sides are made of glass sheets. The V-shaped multi-slit (sharp-crested) weir models were made of 1/16-inch (1.6mm) thick reinforced plexiglas plates with notch angles of 4.58°and 0.57°. The weirs were fixed at the downstream end of the flume (Fig. 3.1) and were fully ventilated. Proper stilling arrangements such as honeycombs and screens were used at the inlet section to ensure a smooth flow in the channel, free from large-scale turbulence. The weir plates were thin enough (1/16 inch) and the flow rates were big enough to avoid the nappe from clinging to the body of the weir plate. There was no need for additional ventilation holes to prevent the clinging of the nappe onto the weir body since air has access all around the nappe for the weir widths considered. On the upstream of the measuring channel, there was a large tank with screens inside to still the water. Thus, it was possible to maintain a disturbance free flow in the channel upstream of the weir. Furthermore, a valve was installed at the most upstream of the set-up to make fine adjustments on the flow rate.

Throughout the experiments, the weir width to channel width ratio (nb/B) covered the range of 0.005 to 0.187. The study covered weirs of many different widths. The weir

height P was constant.

3.2 Experimental Procedure and Data Collection

Before starting experiments, steady state conditions were established by waiting for a period of 30 minutes after starting the water supply to the flume. The range of water temperature was in the range of 20.5-23 °C. The point gage upstream of the weir units was used to measure the free surface height, *H*, above the flume bed level. The gage could measure the flow depth to the nearest 0.1 mm. A 60 degree V notch was normally used to measure the weir flow rate. The heights above the weir, *h (=H-P)* were taken while the volume of flow through the weirs were measured for 60 to100 seconds to calculate small discharge rates for single weir flows. Single weir flows were measured to verify the concept of image weirs. According to this concept, the discharges of each weir of the unit should be nearly the same. Statistically, the relative errors of the discharge measurements are less than 2% in the individual weir discharges measured (Table 2.2).

As such, the measurements were repeated for 6 times at the same *H*, to reduce the influence of flow disturbance and the errors of measuring.

3.3 Cd - Reynolds Number Relation

The data from experiments contain an amount of random measurement errors. To find smooth curves that best fit the data points between variables such as C_d and R_e, the least squares method was used.

According to the previous investigations (Zhai, 2003 and Aydin, 2002), there is a general relationship between C_d and R_e. Thus,

$$C_d = a + b / R_e^{\,n} \tag{3-1}$$

Mathematically, Eq. (3-1) can be generalized as:

$$f(x) = f(x; a_1, a_2, ..., a_m) \tag{3-2}$$

in which $a_1, a_2 ..., a_m$ are parameters to be solved.

For the test data points $(x_i, y_i), i = 1,2,..., n$, there exists:

$$S(a_1, a_2, ..., a_m) = \sum_{i=1}^{n} \left| y_i - f(x_i) \right|^2 \tag{3-3}$$

The optimal values of the parameters are given by

$$\frac{\partial S}{\partial a_k} = 0, k = 1,2,..., m \tag{3-4}$$

For the range of the parameters covered in the present test, the constants *a, b* and *n* of Eq.(3-1) can be obtained. In the next chapter, using test data in Table (3.1), the relationship between C_d and R_{eR} will be shown to be:

$$C_d = 0.575 + (9.71 / R_{eR}^{\,0.52}) \tag{3-5}$$

Here, R_{eR} is the Reynolds number based on characteristic length L equals to twice of hydraulic radius *R*.

Chapter 4

Analysis and Discussion of Results

According to experiments as stated in Chapter 3, the analysis and discussion of results by using present and previous test data are described in this chapter.

4.1 Dimensionless Variables

The geometry of the flow pattern shown in Fig. 2.2 is described by the width of the notch b, the width of the approach channel B, the height of the weir crest p above the bottom of the channel, and the piezometric head h above the level of the crest. The other parameters involved are the specific weight γ, the density ρ, the dynamic viscosity μ, and the surface tension σ. Only one independent flow characteristic is involved, and it can be represented by either the discharge rates Q, or the head h. However, h is already involved as an independent geometric variable, and Q is conveniently selected as the dependent variable. Thus, a complete statement of the discharge function will include both h and Q, as in the following expression:

$$Q = f_1(b, B, P, h, \gamma, \rho, \mu, \sigma) \tag{4-1}$$

From Eq. (2-6), (2-8) and (2-9) for V-shaped multi-slit weir unit, theoretically, the discharge Q through the unit is a function involving the following variables:

$$Q = f_2(b, B, h, P, \theta, \gamma, \mu, \rho, \sigma) \tag{4-2}$$

Here, θ is the dimensionless notch angle and γ is specific weight of water. The other notations are the same as before. Also, here n is the number of active slit weirs that are

functioning.

A dimensional analysis of the variables involved in the discharge rate measurement would lead to a set of dimensionless numbers on which for the multi-slit unit, the discharge coefficient C_d can be expressed by a dimensionless form relating the following parameters:

$$C_d = f_3(\frac{nb}{B}, \frac{nb}{h}, \frac{h}{P}, \theta, R_e, W_e, n) \tag{4-3}$$

because the notch angle θ is a function of b and h, the Eq.(4-3) can be rewritten as,

$$C_d = f_4(\frac{nb}{B}, \frac{nb}{h}, \frac{h}{P}, R_e, W_e) \tag{4-4}$$

From the experimental data, C_d can be obtained from Eq. (2-9):

$$C_d = Q/[\frac{8}{15}(2g)^{0.5} \tan\frac{\theta}{2} h^{2.5}] \tag{4-5}$$

It is clear that the factors influencing the effective discharge coefficient C_d can be divided into two categories: geometry of the flow boundary and flow characteristics of the weirs and the approach channel.

4.2 Influence of Geometric Ratio on Discharge Coefficient (C_d)

In Eq.(4-3), *b/B* is a measure of the contraction characteristics of the weir. In combination with *h/p*, it is also an area-contraction ratio. The influence of *b/B* is similar to that of the corresponding width or diameter ratios which are used to describe the geometry of

orifices. In the present study, this ratio is taken as *(nb)/B*, where n is the number of active slit weirs.

The *b/h* ratio can be described as a shape parameter. The independent influence of this ratio is believed to be negligible over the full practical range of the other variables. In an early investigation, Aydin (2002) supported this hypothesis. The fact that most of the published conclusions of research on single weir ignore *b/h* ratio. They indicate that its influence is not evident from the experimental data. A few recorded efforts to incorporate the *b/h* ratio effect in discharge formulas are believed to be based on misinterpretations of influences related separately to the magnitudes of *b* and *h*.

The *h/p* ratio is a measure of the effect of the approach velocity on the discharge coefficient C_d. Fig. 4.1 shows the variation of C_d with *h/p* for the large *p* values (weir heights) in the present tests, the approach velocity should have little effect on C_d. However, the sketch shows considerable scatter. By considering only points (in the dash line region on Fig. 4.1) associated with larger Reynolds numbers ($R_e \geq 16{,}000$) denoted as solid circles (•), one notice that the high scatter in the C_d-*h/p* diagram is not large.

Fig. 4.2 shows the variation of C_d with *nb/B* for the different values of *n* and *b/B* in the present tests. *nb/B* denotes the effect of the contraction of the weir flow on C_d. Normally, for the choice of low *nb/B* values ($0.005 \leq nb/B \leq 0.187$) in the test, contraction coefficient *Cc* is close to 0.61 and hence should not influence C_d. However, the sketch shows

considerable scatter. By considering only points (in the dash line region on Fig. 4.2) associated with larger Reynolds numbers ($R_e \geq 16{,}000$) denoted as solid circles (•), one notice that the high scatter in the C_d-nb/B diagram is not large.

4.3 Variation of Discharge Coefficient (C_d) with Weber Number (W_e)

The Weber number W_e, which is the ratio of inertial force to surface tension force is a measure of the relative influence of surface tension. It is expressed as follows for open channels. (Olson, 1980)

$$We = \rho V^2 / (\sigma L) \tag{4-6}$$

Here, ρ is the density of water, σ is the surface tension.

Fig. 4.3 shows the variation of the discharge coefficient, C_d, with the Weber number W_e considering all data. The scatter of the data in this presentation is excessive.

In present study, for slit V-shaped weirs, We can be expressed by

$$W_e = 8\rho Q^2 / [\cos(\frac{\theta}{2}) h^2 b^3 \sigma] \tag{4-7}$$

The effect of the occurrence is similar to the effect of rounding the upstream edge of the plate. Therefore, the effect on the discharge is the same as an increase in head.

Because the result of surface tension acting in the direction of the center of curvature of the nappe, the radius of curvature of the nappe surface decreases with decreasing head,

and surface tension force varies increasing by decreasing radius of curvature. It has the same effect on the discharge as an increase in head, so that the influence of surface tension diminishes as the size of the weir and the head increase, and the inertial force dominates.

In the present tests, C_d should not significantly vary with W_e when driving head h is sufficiently large (h>15cm) . However, Fig. 4.3 shows that there is considerable scatter in the C_d-W_e diagram. By considering only points (in the dash line region on Fig. 4.3) associated with larger Reynolds numbers ($R_e \geq 16{,}000$) denoted as solid circles (●), one notice that the high scatter in the C_d-W_e diagram is removed.

4.4 Variation of Discharge Coefficient (C_d) with Reynolds Number(R_e)

The Reynolds number R_e, which is a ratio of the inertia force to the viscous force, is a measure of the relative influence of viscosity. It is usually expressed as follows for an open channel (Gupta, 2001):

$$R_e = \frac{VL}{\nu} \tag{4-8}$$

Here, R_e is the Reynolds number, V is the average velocity; L is the characteristic length and ν is the kinematic viscosity.

Since we have a variable value of the top width b (Fig. 2.7) of the flow area at the notch section for different driving heads h in the case of the V-shaped multi-slit units, we need

to get a different parameter for the characteristic length L in forming the Reynolds number R_e. In open channel flow analysis, L for various channel shapes are generally chosen to be the hydraulic radius $R=A/P=$ (area of flow)/ (wetted perimeter) in determining head loss using Manning's formula. Hence, one can use the hydraulic radius R or a factor of R, say $2R$ as the characteristic length L for R_e for the general slit weir flows. Thus $R_{eR} = \frac{V(2R)}{\nu}$ when L is replaced by $2R$. This permits a general Reynolds number R_{eR} which is valid for rectangular and V-shaped multi-slit weir units. Incidentally, Aydin (2002) used the top width of free water surface on the sharp weirs b as characteristic length L for rectangular slit weirs.

In present study, for V-shaped slit weirs, the Reynolds number R_e based on $L=2R$ can be expressed as follows. (Fig. 2.7)

$$R_{eR} = \cos(\frac{\theta}{2})Q/(h\nu) \tag{4-9}$$

Also, for V-shaped slit weirs, the Reynolds number R_e based on $L=b$ (Aydin, 2002) can be expressed as follows (Fig. 2.7).

$$R_{eb} = Q/(h\nu) \tag{4-10}$$

Here, b denotes the top width of the flow area at the notch section for different driving heads h in the case of the V-shaped multi-slit unit. Fig. 4.4, shows that there is considerable scatter in the C_d - R_{eb} diagram. By considering the Reynolds number based on $L=2R$ as in Eq. (4-9), and plotting C_d as a function of R_{eR}, unified plot with far less scatter can be obtained as in Fig.4.5. The previous correlation between the discharge

coefficient C_d and Reynolds number R_{eR} for single or multiple units of rectangular slit weirs has also been superimposed in Fig.4.5 (solid line). Clearly, the use of the modified Reynolds number R_{eR} appears to be applicable to both rectangular and V-shaped multi-slit weir units. The scatter in the diagram is very small.

4.5 Concept of Image Weir Hypothesis

The weirs on either side of the parent weir are considered to be its images. This hypothesis is supported by the fact that the best fit curve for the multi-slit weir data is essentially the same as the best fit curve for weir units containing 1,3,7 individual weirs. The curve in Figure 4.4 shows a clear dependence of discharge coefficient, C_d, on Reynolds number, R_{eR}. When R_{eR} >40,000, the effects of viscosity are nearly diminished, the line C_d=0.61 appears to be the asymptote to the curve. In other words, the discharge coefficient, C_d, can be represented solely as a function of Reynolds number. When R_{eR} <40,000, there is a slight scatter of the data points which indicate the influence of the other parameter, such as W_e, b/h, h/p and θ.

4.6 Discharge Prediction and Accuracy

To determine the discharge over the multi-slit weir, Eq.(2-9) and Eq. (3-5) must be coupled. In order to calculate the discharge rates for the driving head of the weir, h, and a known multi-slit geometry, iteration is required. The procedure of iterating involves an

arbitrarily assumed discharge rate Q and the use of Eq. (4-7) to obtain the corresponding R_{eR} and correct it. Converges occurs within a few iteration. The result of discharge prediction and its accuracy are shown in Table 4.1, in which the root mean error is 0.03 L/s and 97% of data is within the 3.5% of the values predicted by Eq. (3-5). Fig. 4.6 shows the relation between measured C_d and calculated C_d fall within the 95% confidence interval. For very small value of R_e, *h/b, h/p* ratio, the effect of surface tension was dominated so that the reliable measurements could not be made and the relative error should be bigger than others.

In general, Eq. (2-9) can be written for various weirs as:

$$Q = Kh^u \tag{4-11}$$

Where K depends on C_d and geometry parameters of weirs, u=2.5 and 1.5 for V-notch and rectangular weirs separately.

Typically, in the (shaped edged) V-shaped weir (or notch), the discharge rate Q_1, with the head h_1 raised to the power of 2.5. That is $Q_{1-V-shapedweir} \propto h_1^{2.5}$, for (sharp edged) rectangular weir (or notch), $Q_{1-rectangularweir} \propto h_1^{1.5}$.

In a typical laboratory setting, the tank in which the weir (or notch) is located permits one to measure discharge rate Q accurately in the fixed range of heads h_1 to h_2.

For instance, it can be noted that the minimum head for proper discharge rate measurement, one uses the minimum head h_1 of 150 mm to avoid surface tension effect [Sarginson 1972]. Let h_2=500mm to be the largest head that can be accurately measured. Hence, for this condition, the corresponding largest discharge measured Q_2 will be $Q_1 \times (\frac{500}{150})^{2.5} = 20.3Q_1$. Similarly, one notes that for a rectangular notch, the maximum discharge rate $Q_2^{'}$ measure at a head h_2=500mm is $Q_1^{'} \times (\frac{500}{150})^{1.5} = 6.1Q_1^{'}$. As such, the V-shaped weir (or notch) permits one to cover a much wider range of the discharge rates than a rectangular weir (or notch). It may be noted that V notches are commonly used for laboratory discharge rate (Q) measurement where the Q range is very large.

Chapter 5

Summary, Conclusions and Scope for Future Study

Summary

A generalized Reynolds number R_{eR} applicable to both rectangular and V-shaped multi-slit weir units is proposed. For this, the hydraulic radius R based on the ratio of the flow area to the wetted perimeter of the flow area at the multi-slit weir section is used to form R_{eR}. Test data are used to validate the concept of image weirs. A very brief CFD study is made to predict some flow features of the multi-slit weir flow.

5.1 Conclusions

1) A properly constructed test facility permits one to test and validate the hypothesis that the weirs on either side of the parent weir can be considered to be images of the parent weir.
2) Multi-slit (sharp-crested) weirs can be used to accurately measure a very wide range of flow rates. For example, the V-shaped weirs with notch angle, θ= 4.58 degrees and notch number n=7 can measure a range of 54.6 L/s to 0.3 L/s (n=1). This denotes a factor of nearly 200 for the minimum and maximum discharge rate values.
3) For the range of weir parameters selected in the present (V-shaped multi-slit weir units) and previous (rectangular multi-slit weir units) studies, the discharge

coefficient C_d solely varies with the Reynolds number R_{eR}.

4) For R_{eR}>40,000, the line C_d=0.61 appears to be the asymptote to the curve. This corresponds to the correction coefficient in the C_d - R_e curve value of Cc for a narrow slit.

5) The present short study using CFD modeling approach indicate that simulation can be effectively applied for the describing the characteristics of flow past a multi-slit weir units in open channels.

5.2 Scope for Future Study

1) Other shapes of multi-slit weir units can be tested to form multi-slit weir units and the applicability of R_{eR} may be examined for them.

2) The use of multi-slit weir which forms a flow control in the downstream (or outlet) of flumes can be studied, as the flow upstream of multi-slit weir unit will be more uniform than a single wide weir.

References:

1. Ahmed, F.H.(1985). "Characteristics of Discharge of the Combined Flow through Sluice Gate and Over Weirs", Journal Engineering and Technology, Iraq, Vol 3, No. 2, pp 49-63.
2. Aydin, I., Ger, A. M. and Hincal, O. (2002). "Measurement of Small Discharge in Open Channels by Slit Weir", Journal of Hydraulic Engineering, ASCE, 128 (2), pp 234-237.
3. Bauer, S. and Graf, W., "Free Overfall as Flow Measuring Derive", Journal of Irrigation and Drainage Division, ASCE, Vol. 97, No IR1, March, 1971, pp 73-83
4. Bos, M. G. (1989). "Discharge Measurement Structures", 3rd Ed., International Institute for Land Reclamation and Improvement/ILRI, Wageningen, Netherlands.
5. Chao Zhai (2003). "Application of Some Hydraulic Principles to Flow Measurement", M.A.Sc thesis, Faculty of Engineering and Computer Science, Concordia University, Montreal, QC, Canada..
6. Chen Q., Dai G. and Liu H. (2002). "Volume of Fluid Model for Turbulence Numerical Simulation of Stepped Spillway Overflow of

Plane Free Overfall", Journal of Hydraulic Engineering, ASCE, 128(7), pp 683-688.

7. Chow, V. T. (1959). "Open Channel Hydraulics", McGraw-Hill, New York.

8. Fathy, A. and Shaarawi, M., "Hydraulics of The Free Overfall", Proceeding, ASCE, Vol.80, Proceeds paper No.564, Dec 1954, pp 564-1-564-12.

9. Ferziger, J. H. and Peric M. (2002). "Computational Method for CFD", 3rd edition, Springer.

10. Gupta, R.D., Jamil, M., and Mohsin, M., "Discharge Prediction in Smooth Trapezoidal Free Overfall", Journal of Irrigation and Drainage Engineering, ASCE, Vol. 119, No.2 1993, pp 215-224.

11. Gerald, C. F. and Wheatley, P. O. (1994). "Applied Numerical Analysis", 5th edition, Addison-Wesley Publishing Company.

12. Hager, W.H., "Hydraulics of Plane Free Overfall", Journal of Hydraulic Engineering, ASCE, Vol. 109, No. 12, Dec., 1983, pp 1683-1697.

13. Han, T.Y. and Chow, W.L., "The Study of Sluice Gates and Sharp-Crested Weirs through Hodograph Transformations", Journal of Applied Mechanics, ASME, Vol.48, June 1981, pp 229-234.

14. Huang, J. (2000). "Development and Validation of a Three-Dimensional Numerical Model for Application to River Flow", Ph.D thesis, Faculty of Civil Engineering, University of Iowa, Iowa, U.S. A.

15. Huang, J., Weber, L. J and Lai, Y. G. (2002). "3D Numerical Study of Flows in Open-Channel Junctions", Journal of Hydraulic Engineering, ASCE, 128(3), pp 268-280.

16. Kandaswamy, P. K. and Rouse, H. (1957). "Characteristics of Flow Over Terminal Weirs and Sills", Journal of the Hydraulic Division, ASCE, 83 (4), pp 1-13.

17. Kindsvater, C. E., and Cater, R.W. (1957). "Discharge Characteristics of Rectangular Thin-Plate weirs", Journal of the Hydraulic Division, ASCE, 83(6), pp 1-36.

18. Meselhe, E. A. and Sotiropoulos, F. (2000). "Three-Dimensional Numerical Model for Open Channels with Free-Surface Variations", Journal of Hydraulic Research, IAHR, 38(2), pp 115-121.

19. Negm, A.M., El-Saiad, A.A., Alhamid, A.A., and Husain, D. (1994), "Characteristics of Simultaneous Flow Over Weir and Below Inverted V-Notches", Civil Engineering Research Magazine (CERM), Civil Engineering Department, Faculty of Engineering, Al-Azhar University, Cairo, Egypt, Vol. 16, No. 9, pp 786-799.

20. Olson, M.G. "Engineering Fluid Mechanics", 2nd Ed., International Textbook Company, Pennsylvania, 1968.

21. Qu Junying(2005), "Three-Dimension Turbulence Modeling for Free Surface Flows", Ph.D thesis, Faculty of Engineering and Computer Science, Concordia University, Montreal, QC, Canada.

22. Rajaratnam, N. and Muralidhar, D., "Characteristics of the Rectangular Free Overfall", Journal of Hydraulic Research, ASCE, Vol. 6, No.3 1968, pp 233-258.

23. Ramamurthy.A.S., Udoyara, S.Tim and Rao M.V.J., "Flow over Sharp-Crested Plate Weirs", Journal of Irrigation and Drainage Engineering, ASCE, Vol. 113, No.2, 1987, pp 163-172.

24. Rameshwaran, P. and Naden, P. S. (2003). "Three-Dimensional Numerical Simulation of Compound Channel Flows", Journal of Hydraulic Engineering, ASCE, 129(8), pp 645-652.

25. Rouse, H. (1950). "Engineering Hydraulics", John Wiley & Sons Inc., New York.

26. Sarginson, E.J., "The Influence of Surface Tension on Weir Flow", Journal of Hydraulic Research, Vol. 10, 1972, pp 431-446.

27. Subhash C.Jain., "Open Channel Flow", John Wiley & Sons Inc., New York, 2000.

28. Vallentin H.R., "Applied Hydrodynamics", Butterworths, London, 1967.

29. Wilcox, D. C. (1994). "Simulation of Transition with a Two-Equation Turbulence Model", AIAA Journal, 32(2), pp 247-255.

30. Wilcox, D. C. (2000). "Turbulence Modeling for CFD". 3rd edition, DCW Industries, Inc. U.S.A.

Table 2.1 **Range of Dimensionless Variables for V-shaped Multi-slit Weirs**

Dimensionless Variable	Minimum Value	Maximum Value
R_{eR}	1304	37384
W_e	12.8	1278.5
h/b	1.36	110
nb/B	0.005	0.187
h/p	0.19	9.76

T=20.5-23°C

Table 2.2 Direct Measurement of Flow Rates through an Individual Slit Weir of V-shaped Multi-slit Weir Unit

Slit No.	Q_i (L/s)	Error %
1	1.195	1.1
2	1.166	-1.35
3	1.188	0.51
4	1.172	-0.85
5	1.189	0.59
6	1.167	-1.23
7	1.201	1.6

T=22°C

n=7,

Total Discharge Q= 8.28 L/s

No.4 is the parent weir; No. 1,2,3,5,6,7 are image weirs.

Table 3.1 **V-shaped Multi-Slit Weirs Data Analysis**

(Temperature ranges: 20.5°C to 23°C ± 0.1°C--Actual temperatures during test are used)

No.	Active Slits n	Slit Width b (mm)	Notch Angle θ	Hydraulic Radius R (mm)	nb/B	Driving Head h (mm)	h/p	h/nb	C_d	We	Reb	Re_R
1	1	2.8	0.57	0.70	0.005	281.4	0.42	100	0.786	13.8	2698	1356
2	1	15.1	4.58	3.78	0.025	188.3	0.28	12.5	0.668	48.1	12831	6448
3	1	16.3	4.58	4.08	0.027	203.7	0.3	12.5	0.663	55.1	14275	7173
4	1	19.3	4.58	4.83	0.032	241.2	0.36	12.5	0.653	75.3	18176	9134
5	1	19.8	4.58	4.95	0.033	250.6	0.37	12.5	0.65	80.6	19161	9628
6	1	21	4.58	5.25	0.035	259.3	0.39	12.5	0.645	84.5	19936	10018
7	1	21.7	4.58	5.43	0.036	270.7	0.4	12.5	0.644	92.2	21307	10707
8	1	22.2	4.58	5.55	0.037	278.1	0.42	12.5	0.644	97	22127	11119
9	1	22.8	4.58	5.70	0.038	282.1	0.42	12.5	0.643	99.7	22597	11355
10	1	23.4	4.58	5.85	0.039	292.1	0.44	12.5	0.642	106.5	23770	11945
11	1	29.4	4.58	7.35	0.049	367.8	0.55	12.5	0.64	167.4	33429	16799
12	1	29.4	4.58	7.35	0.049	369.8	0.55	12.5	0.634	166.5	33449	16808
13	1	30.6	4.58	7.65	0.051	381.2	0.57	12.5	0.624	171.4	34441	17307
14	1	30.6	4.58	7.65	0.051	381.2	0.57	12.5	0.632	175.6	34871	17523
15	1	30.6	4.58	7.65	0.051	381.2	0.57	12.5	0.635	177.9	35113	17645
16	1	30.6	4.58	7.65	0.051	381.9	0.57	12.5	0.634	177.9	35135	17656
17	1	31.8	4.58	7.95	0.053	397.3	0.59	12.5	0.626	187.4	36787	18486
18	1	32.4	4.58	8.10	0.054	406.7	0.61	12.5	0.623	194.1	37862	19026
19	1	3.2	0.57	0.80	0.005	321.6	0.48	110	0.743	24	4201	2111
20	3	2.6	0.57	0.65	0.013	261.3	0.39	33.33	0.755	12.8	2595	1304
21	3	3.7	0.57	0.93	0.019	371.2	0.55	33.33	0.808	31	4880	2452
22	3	3.8	0.57	0.95	0.019	376.5	0.56	33.33	0.803	31.5	4951	2488
23	3	1.3	0.57	0.33	0.007	131.3	0.2	33.33	0.705	25.9	7844	3942
24	3	1.7	0.57	0.43	0.008	167.5	0.25	33.33	0.678	39.1	10909	5482

Table 3.1 (Continued) **V-shaped Multi-Slit Weirs Data Analysis**

(Temperature ranges: 20.5°C to 23°C ± 0.1°C--Actual temperatures during test are used)

No.	Active Slits n	Slit Width b (mm)	Notch Angle θ	Hydraulic Radius R (mm)	nb/B	Driving Head h (mm)	h/p	h/nb	C_d	We	Reb	Re_R
25	3	1.7	0.57	0.43	0.008	168.8	0.25	33.33	0.674	39.2	10959	5507
26	3	22.7	4.58	5.68	0.113	283.4	0.42	12.5	0.628	95.8	22200	11156
27	3	3.6	0.57	0.90	0.018	355.8	0.53	110	0.761	25.2	4304	2163
28	3	15	4.58	3.75	0.075	188.3	0.28	4.2	0.674	48.9	12945	6505
29	3	16.4	4.58	4.10	0.082	203.7	0.3	4.16	0.664	55.6	14355	7214
30	3	19.4	4.58	4.85	0.097	241.2	0.36	4.17	0.654	75.6	18207	9149
31	3	20	4.58	5.00	0.1	250.6	0.37	4.18	0.655	81.9	19311	9704
32	3	19.3	4.58	4.83	0.097	258.6	0.39	4.17	0.645	84.3	19903	10002
33	3	16.3	4.58	4.08	0.082	265.3	0.4	4.16	0.652	90.9	20932	10519
34	3	19.3	4.58	4.83	0.097	268	0.4	4.17	0.654	93.1	21290	10699
35	3	22	4.58	5.50	0.11	275.4	0.41	4.18	0.65	97.2	22058	11084
36	3	22	4.58	5.50	0.11	275.4	0.41	4.18	0.653	98.1	22154	11133
37	3	22.8	4.58	5.70	0.114	284.8	0.43	4.19	0.651	104	23203	11660
38	3	25.2	4.58	6.30	0.126	314.2	0.47	4.19	0.633	119.5	26105	13118
39	7	2.9	0.57	0.73	0.034	294.8	0.44	14.29	0.834	15.6	2864	1439
40	7	3.4	0.57	0.85	0.039	335	0.5	14.29	0.776	28.6	4685	2354
41	7	3.8	0.57	0.95	0.044	376.5	0.56	14.29	0.761	28.3	4692	2358
42	7	1.3	0.57	0.33	0.015	126	0.19	14.29	0.723	25.1	7581	3810
43	7	1.5	0.57	0.38	0.018	151.4	0.23	14.29	0.67	31.2	9267	4657
44	7	22	4.58	5.50	0.036	275.4	0.41	12.5	0.651	97.5	22086	11098
45	7	3.6	0.57	0.9	0.042	355.8	0.53	110	0.748	24.4	4230	2126
46	7	16	4.58	4.00	0.187	203.7	0.3	1.82	0.671	56.8	14510	7291
47	7	16	4.58	4.00	0.187	203.7	0.3	1.82	0.674	57.3	14566	7320

Table 3.1 (Continued) **Rectangular Multi-Slit Weirs Data Analysis**

(Temperature ranges: 20.5°C to 23°C ± 0.1°C--Actual temperatures during test are used)

No.	Active Slits n	Slit Width b (mm)	Hydraulic Radius R (mm)	nb/B	Driving Head h (mm)	h/p	h/nb	C_d	We	Reb	Re_R
1	1	5	2.48	0.008	387.4	0.66	77.9	0.686	105.7	6302	6262
2	1	10	4.89	0.017	223.1	0.38	22.1	0.672	119.3	9293	9087
3	1	10	4.92	0.017	305.2	0.52	30.7	0.665	162.4	10842	10668
4	1	10	4.93	0.017	375.7	0.64	37.29	0.656	192.2	11796	11640
5	1	10	4.94	0.017	434.4	0.74	43.2	0.65	218.6	12570	12426
6	1	36	14.50	0.118	74.5	2.07	2.07	0.64	133.2	18628	15004
7	1	36	17.86	0.118	2251.2	3.36	3.36	0.64	216.5	23750	20674
8	1	36	13.94	0.118	61.9	1.72	3.82	0.64	240.2	25020	22124
9	1	36	16.16	0.118	158	4.39	4.39	0.636	275.1	26774	24036
10	1	36	16.49	0.118	196.2	5.45	5.45	0.628	336.7	29621	27132
11	1	36	15.00	0.118	90	2.5	5.56	0.627	341.4	29826	27365
12	1	36	16.74	0.118	239.4	6.65	6.65	0.627	407.1	32571	30293
13	1	36	15.46	0.118	109.4	3.04	6.76	0.627	413.9	32844	30582
14	1	36	15.66	0.118	120.6	3.35	7.44	0.62	450.7	34270	32112
15	1	36	17.14	0.118	358.1	0.61	1.36	0.65	88.5	15189	11106
16	1	36	16.93	0.118	283.7	7.88	7.88	0.62	481.2	35410	33297
17	1	36	15.67	0.118	121	3.36	8.21	0.626	502.3	36179	34102
18	1	36	15.95	0.118	140	3.89	8.62	0.625	529	37127	35092
19	1	36	17.05	0.118	321.5	8.93	8.93	0.625	547	37753	35751
20	1	36	17.12	0.118	351.4	9.76	9.76	0.625	592.7	39299	37384
21	3	5	2.46	0.025	158.5	0.27	31.9	0.713	139.8	4191	4126

Table 3.1 (Continued) **Rectangular Multi-Slit Weirs Data Analysis**

(Temperature ranges: 20.5°C to 23°C ± 0.1°C--Actual temperatures during test are used)

No.	Active Slits n	Slit Width b (mm)	Hydraulic Radius R (mm)	nb/B	Driving Head h (mm)	h/p	h/nb	C_d	We	Reb	Re_R
22	3	10	4.79	0.05	111.5	0.19	10.97	0.69	187.3	6723	6430
23	3	10	4.86	0.05	176.1	0.3	17.7	0.674	288.6	8344	8115
24	3	10	4.89	0.05	217.2	0.37	21.88	0.671	353.9	9241	9035
25	3	10	4.91	0.05	275.9	0.47	27.67	0.669	445.1	10363	10179
26	3	10	4.93	0.05	328.7	0.56	32.85	0.666	523.1	11235	11067
27	3	10	4.93	0.05	375.7	0.64	37.58	0.664	595.7	11989	11832
28	7	5	2.45	0.054	111.5	0.19	22.06	0.728	227.8	3557	3478
29	7	5	2.46	0.054	152.6	0.26	30.7	0.709	313.8	4088	4022
30	7	5	2.47	0.054	240.7	0.41	47.64	0.696	472.4	4999	4947
31	7	5	2.48	0.054	311.1	0.53	61.82	0.692	596.4	5662	5617
32	7	5	2.48	0.054	387.4	0.66	77.76	0.687	754.9	6301	6261
33	7	10	4.90	0.117	234.5	0.35	20.79	0.674	791.4	9046	8834
34	7	10	4.93	0.117	341.7	0.51	29.87	0.671	1127.7	10799	10621
35	7	15	7.19	0.175	174.2	0.26	30.26	0.653	810.3	11211	11029
36	7	15	7.24	0.175	207.7	0.31	36.84	0.656	995.2	12424	12258
37	7	15	7.25	0.175	214.4	0.32	37.7	0.659	1027.4	12624	12459
38	7	15	7.27	0.175	241.2	0.36	42.18	0.654	1133.8	13262	13107
39	7	15	7.30	0.175	274.7	0.41	48.22	0.65	1278.5	14083	13938
40	7	15	7.33	0.175	321.6	0.48	56.08	0.642	1073	15015	14882
41	15	5	2.46	0.125	160.8	0.24	28.3	0.713	589.9	3949	3880
42	15	5	2.47	0.125	221.1	0.33	38.16	0.699	820.5	4492	4434
43	15	5	2.48	0.125	321.6	0.48	56.44	0.694	1200.9	5424	5376

Table 4.1 Prediction of Discharge Q of V-shaped Multi-slit Weirs

H (mm)	h (mm)	Q_1 (cm^3/s)	Re_R	C_d	Q_2 (cm^3/s)	Q_2-Q_1 (cm^3/s)	Error%
874	204	1160	7093	0.672	1194	34	2.91
805	135	382	3825	0.667	392	10	2.62
945.5	275.5	2470	11184	0.652	2455	-15	0.61
911.5	241.5	1801	9303	0.66	1787	-14	0.75
954.9	284.9	2649	11601	0.651	2665	16	0.62
781.5	111.5	280	3132	0.724	284	4	1.40
779.5	109.5	265	3018	0.727	272	7	2.83
837.5	167.5	736	5482	0.687	746	10	1.33
843.8	173.8	791	5678	0.685	815	24	3.01
873.5	203.5	1170	7173	0.672	1186	16	1.36
904.6	234.6	1629	8662	0.663	1669	40	2.47
955.8	285.8	2609	11386	0.651	2687	78	3.01
974	304	3035	12454	0.648	3122	87	2.86
1016	346	4180	15070	0.641	4266	87	2.07
1052	382	5407	17656	0.636	5424	17	0.32
1076	406	6200	19026	0.633	6299	99	1.60
1118.2	448.2	7734	21524	0.629	7988	254	3.28
1120	450	7758	21501	0.629	8079	321	4.14

T=20.5-23°C

Q_1 = measured discharge, (cm^3/s)

Q_2 = predicted discharge, (cm^3/s)

Table A.1 **Geometric Weir Parameters and Grid Cells**

(Time step=0.005 second)

Line	IR	JR	JK	HI	AH	BK	HN	KO	HL	KM
Cells	40	40	20	20	71	71	40	40	40	40
Ratio	1.0	1.0	1.0	1.0	0.98	0.98	1.0	1.0	1.0	1.0

Table A.2 Simulation of Central Line Water Surface Profiles for V-shaped Weir in an Open Channel (z=0.61m; Q_r = 31.4 L/s, T= 20.5-23°C)

x (m)	y (m)		x (m)	y (m)		x (m)	y (m)
0.005	0.681		0.541	0.674		1.004	0.665
0.012	0.668		0.557	0.665		1.084	0.668
0.18	0.668		0.583	0.668		1.093	0.671
0.189	0.671		0.603	0.67		1.11	0.669
0.249	0.672		0.658	0.67		1.141	0.671
0.262	0.667		0.667	0.669		1.175	0.67
0.28	0.673		0.682	0.677		1.26	0.674
0.302	0.675		0.694	0.672		1.279	0.675
0.353	0.668		0.704	0.678		1.293	0.677
0.355	0.667		0.736	0.673		1.294	0.665
0.384	0.683		0.746	0.671		1.352	0.679
0.405	0.68		0.749	0.674		1.48	0.666
0.413	0.675		0.768	0.678		1.505	0.669
0.467	0.668		0.787	0.671		1.512	0.667
0.472	0.674		0.795	0.678		1.512	0.677
0.496	0.683		0.85	0.682		1.529	0.68
0.514	0.665		0.909	0.667		1.556	0.676
0.517	0.668		0.909	0.667		1.597	0.667
0.52	0.667		0.951	0.667		1.61	0.671
0.54	0.68		0.975	0.679		1.644	0.667

Table A.2 (Continued)

Simulation of Central Line Water Surface Profiles for V-shaped Weir in an Open Channel (z=0.61m; Q_r = 31.4 L/s, T=20.5-23°C)

x (m)	y (m)		x (m)	y (m)		x (m)	y (m)
1.671	0.666		2.169	0.679		2.859	0.67
1.714	0.674		2.197	0.668		2.87	0.668
1.781	0.667		2.203	0.671		2.924	0.667
1.781	0.667		2.29	0.68		2.948	0.676
1.794	0.675		2.294	0.672		2.985	0.669
1.797	0.667		2.301	0.677		2.985	0.671
1.819	0.671		2.343	0.667		2.988	0.247
1.881	0.68		2.343	0.667		2.995	0.256
1.89	0.666		2.365	0.676		2.997	0.263
1.902	0.68		2.419	0.667		2.998	0.656
1.919	0.67		2.431	0.67		2.998	0.662
1.92	0.678		2.431	0.669		2.999	0.271
1.945	0.672		2.505	0.664		3.002	0.303
1.971	0.668		2.538	0.671		3.003	0.653
2.016	0.666		2.56	0.668		3.006	0.285
2.048	0.667		2.632	0.671		3.008	0.291
2.059	0.68		2.653	0.673		3.009	0.653
2.063	0.673		2.699	0.666		3.012	0.296
2.108	0.68		2.752	0.668		3.014	0.637
2.143	0.674		2.823	0.67		3.016	0.633

Table A.2 (Continued)

Simulation of Central Line Water Surface Profiles

for V-shaped Weir in an Open Channel
(z=0.61m; Q_r = 31.4 L/s, T= 20.5-23°C)

x (m)	y (m)		x (m)	y (m)		x (m)	y (m)
3.017	0.301		3.089	0.326		3.192	0.329
3.019	0.645		3.089	0.607		3.192	0.326
3.027	0.306		3.095	0.6		3.196	0.488
3.032	0.637		3.096	0.585		3.203	0.473
3.035	0.311		3.106	0.58		3.203	0.32
3.041	0.619		3.108	0.337		3.211	0.316
3.042	0.629		3.121	0.338		3.215	0.462
3.044	0.313		3.123	0.569		3.215	0.313
3.047	0.608		3.139	0.337		3.22	0.452
3.054	0.318		3.141	0.555		3.224	0.308
3.056	0.605		3.146	0.545		3.233	0.437
3.06	0.619		3.151	0.338		3.236	0.429
3.066	0.6		3.159	0.527		3.238	0.296
3.069	0.319		3.159	0.338		3.245	0.289
3.075	0.622		3.169	0.338		3.246	0.422
3.078	0.594		3.173	0.513		3.249	0.286
3.078	0.61		3.178	0.335		3.252	0.416
3.08	0.32		3.18	0.505		3.256	0.281
3.082	0.588		3.187	0.496		3.259	0.402
3.083	0.604		3.187	0.332		3.26	0.278

Table A.2 (Continued)

Simulation of Central Line Water Surface Profiles

for V-shaped Weir in an Open Channel
(z=0.61m; Q_r = 31.4 L/s, T=20.5-23°C)

x (m)	y (m)	x (m)	y (m)	x (m)	y (m)
3.262	0.394	3.323	0.215	3.376	0.134
3.264	0.272	3.324	0.3	3.38	0.122
3.271	0.38	3.328	0.288	3.381	0.212
3.271	0.269	3.333	0.205	3.385	0.205
3.277	0.373	3.336	0.282	3.388	0.111
3.281	0.263	3.343	0.194	3.392	0.196
3.283	0.365	3.346	0.274	3.393	0.103
3.283	0.26	3.348	0.185	3.394	0.188
3.288	0.354	3.349	0.289	3.397	0.094
3.289	0.253	3.352	0.265	3.401	0.162
3.294	0.343	3.353	0.174	3.401	0.087
3.294	0.247	3.358	0.252	3.402	0.179
3.3	0.332	3.359	0.165	3.404	0.076
3.3	0.243	3.362	0.244	3.407	0.171
3.303	0.243	3.365	0.154	3.415	0.154
3.303	0.238	3.367	0.238	3.421	0.152
3.307	0.321	3.372	0.229	3.424	0.143
3.311	0.226	3.372	0.147	3.428	0.134
3.312	0.312	3.374	0.14	3.429	0.117
3.316	0.22	3.375	0.22	3.432	0.127

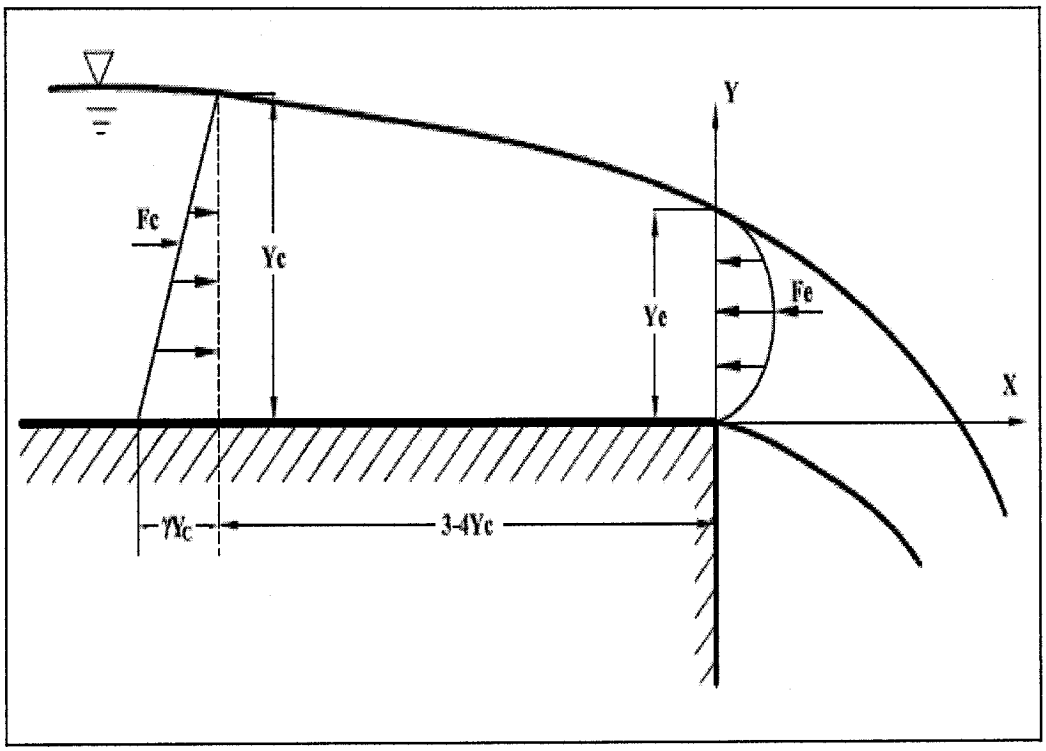

Fig. 1.1 Pressure Distribution in the Approach Channel at the Brink Section

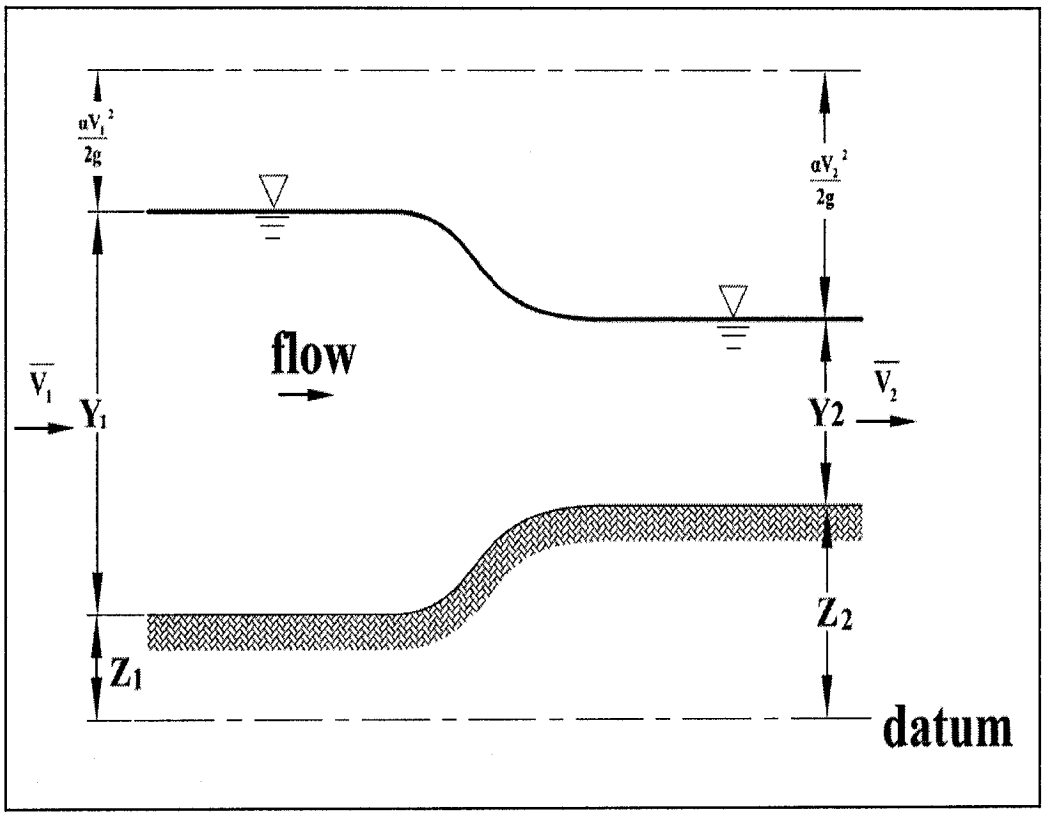

Fig. 2.1 Channel Transition

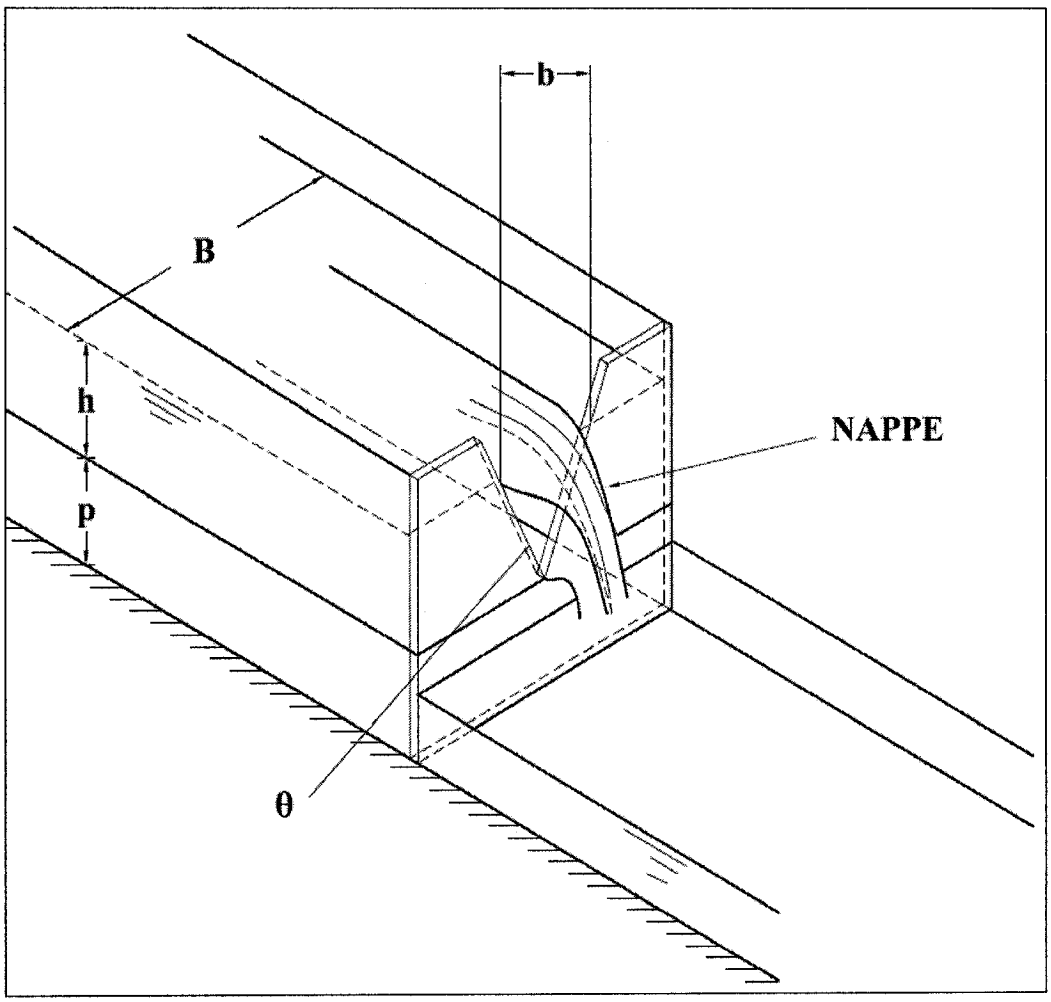

P = Height of The Tip of Notch Above Channel Floor;

B = Channel Width;

h = Head Causing Flow;

θ = Angle of Notch.

Fig. 2.2 Sharp-crested V-notch Sketch

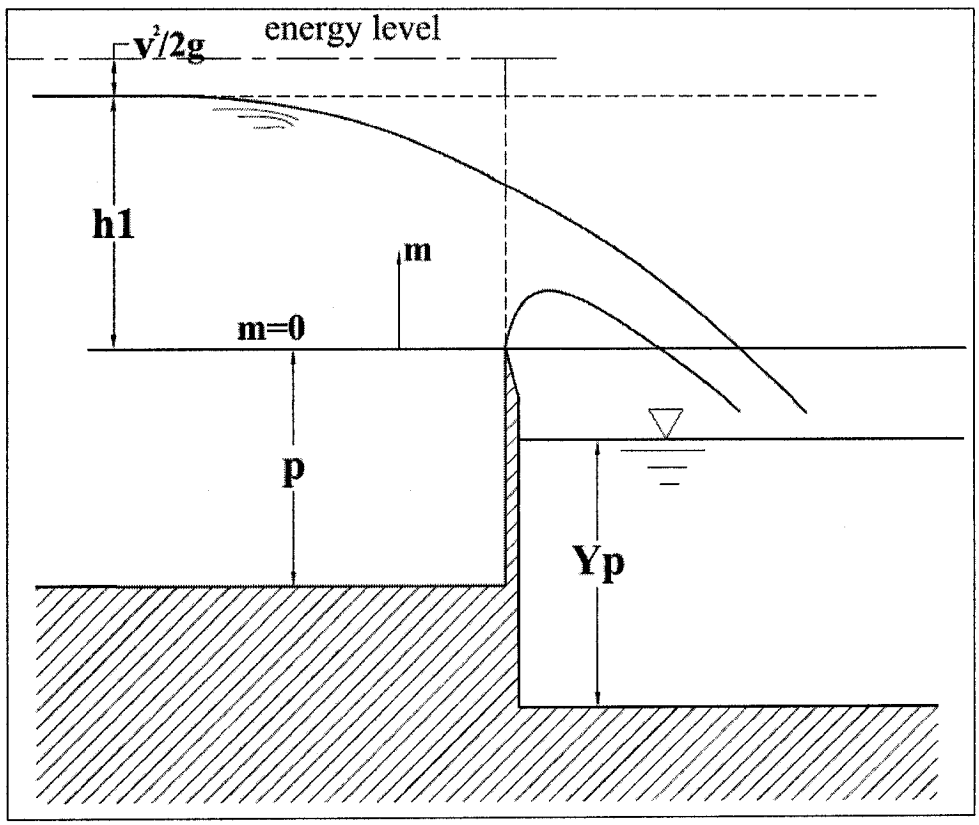

Fig. 2.3 Parameters of Sharp-crested Weir

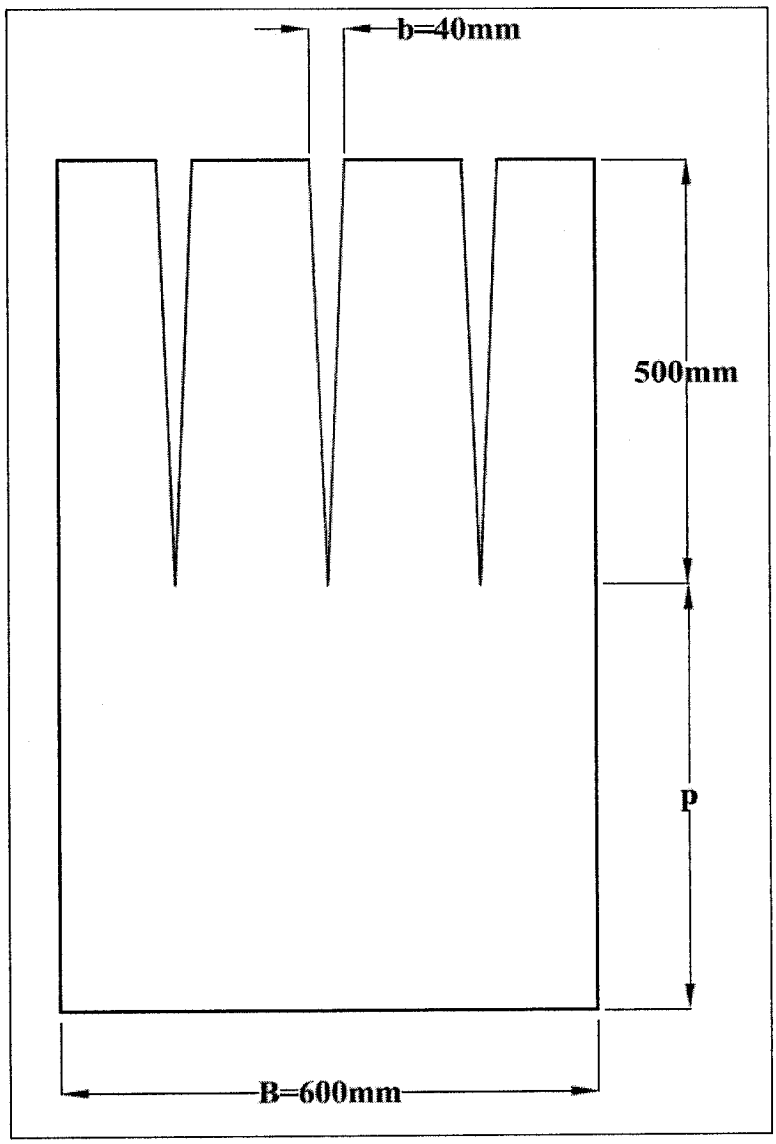

Weir Unit 1: b=40 mm, θ=4.58°;
Weir Unit 2: b=5mm, θ=0.57°;
θ= Notch Angle.

Fig. 2.4 V-shaped Multi-slit Weir (n=3)

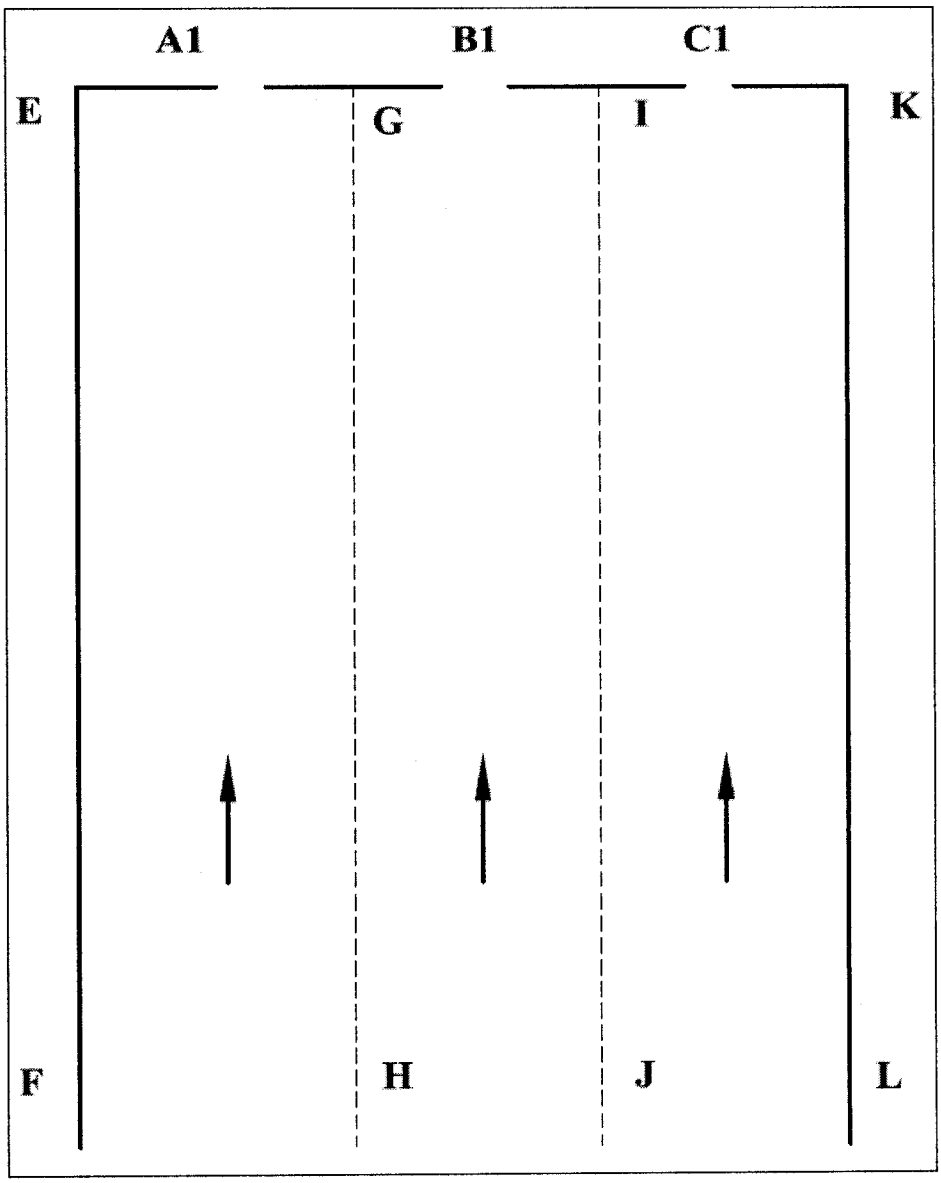

B1=Parent weir;
A1, C1=Image weirs
HG, JI=Stagnation Streamlines

Fig. 2.5a Stagnation Streamlines for Slit Weir Unit (Number of Weirs = 3)

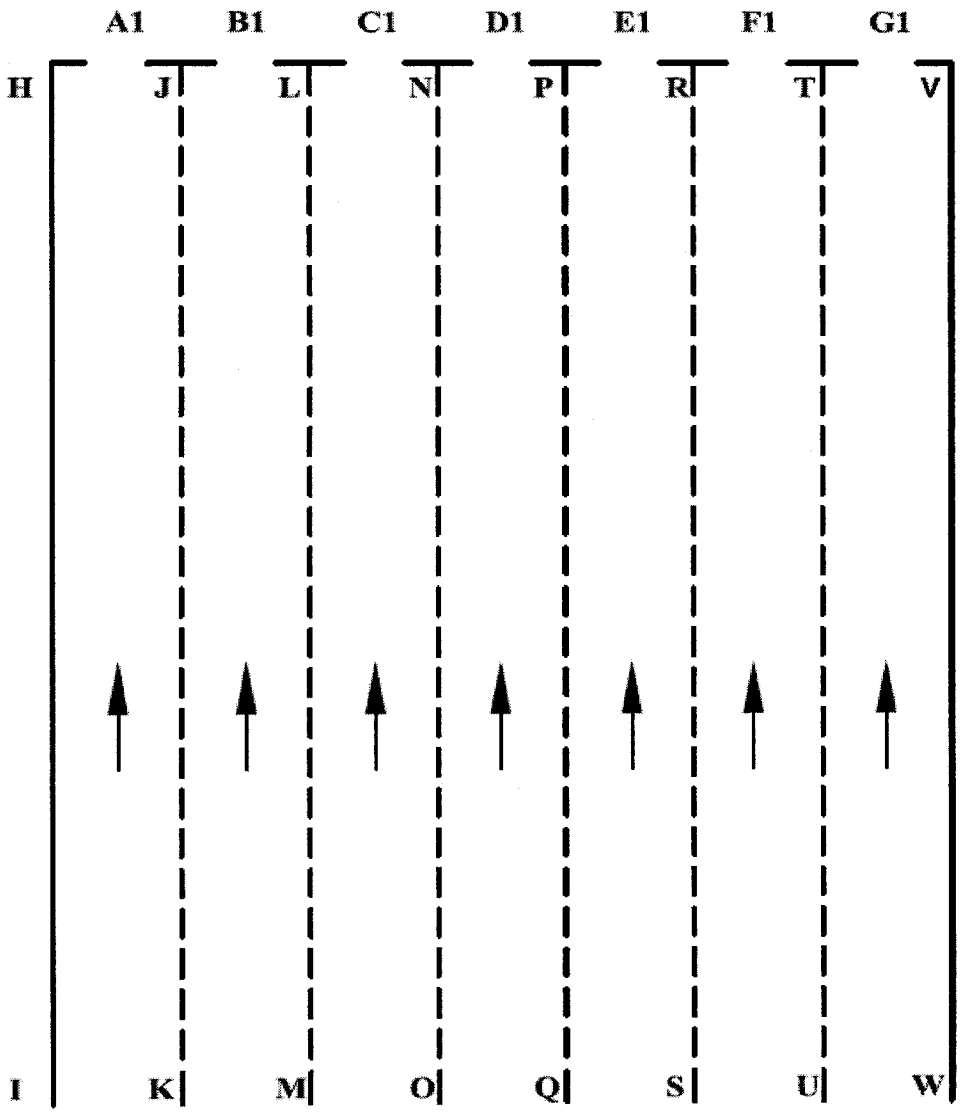

D_1=Parent weir
A_1, B_1, C_1, D_1, E_1, F_1, and G_1=Image weir
KJ, ML, ON, QP, SR, UT, WV= Stagnation Streamlines

Fig.2.5b Stagnation Streamlines for Slit Weir Unit (Number of Weirs = 7)

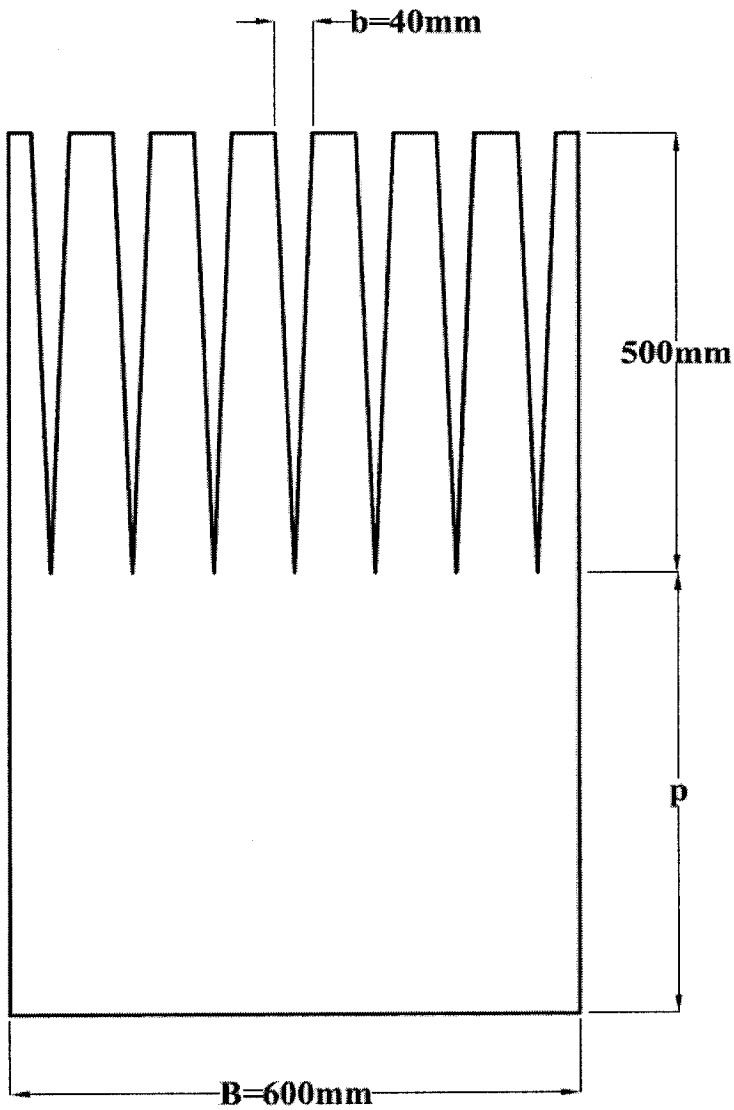

Weir Unit 1: b=40 mm, θ=4.58°;
Weir Unit 2: b=5mm, θ=0.57°.
θ= Notch Angle.

Fig. 2.6 V-shaped Multi-slit Weir (n=7)

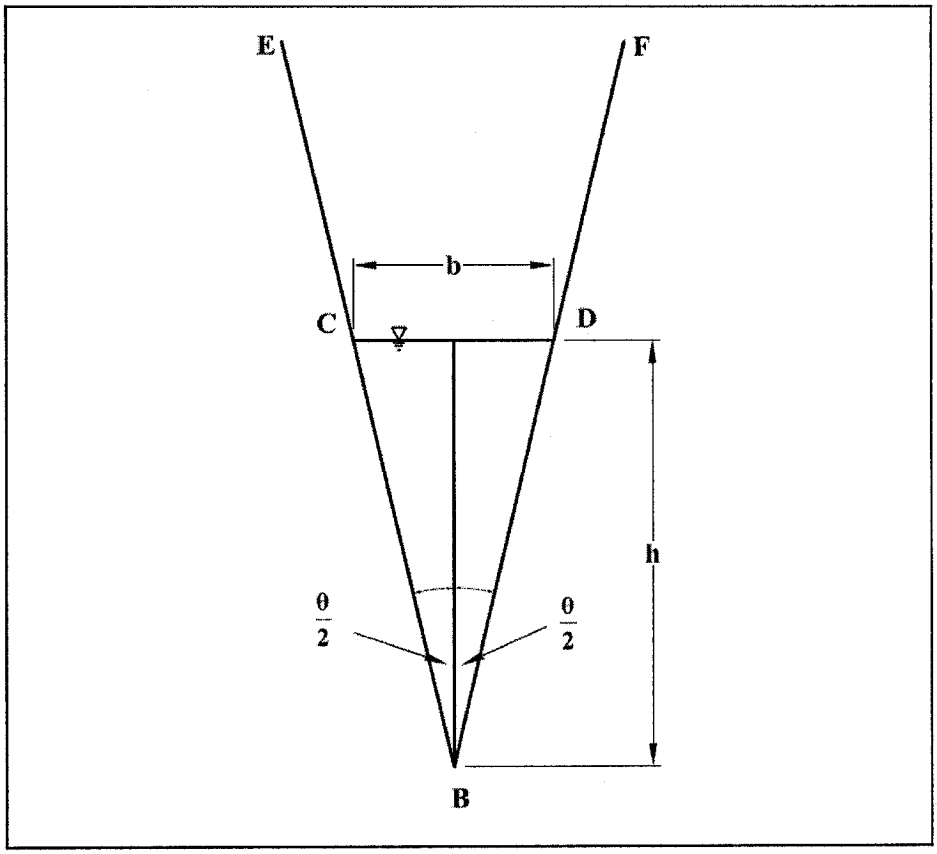

Here,

Witted Perimeter P = BC+BD;

Area of Weir Section A = b*h/2;

Hydraulic Radius R = P/A.

Fig.2.7 Hydraulic Concept of Single V-shaped Weir

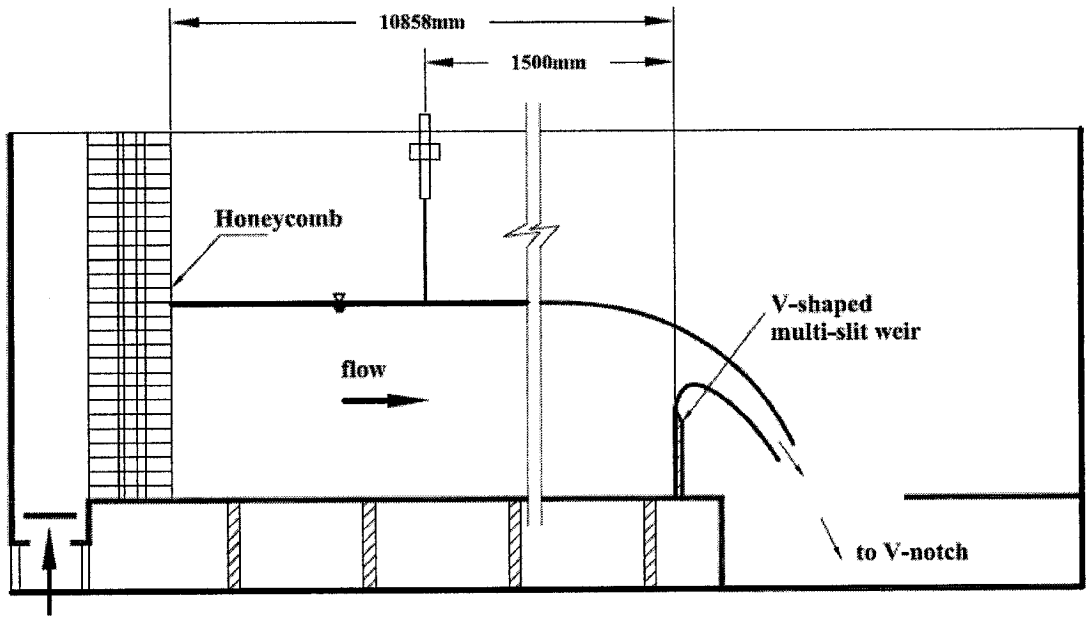

Fig. 3.1 Experimental Set-up for Multi-slit V-shaped Weir Study

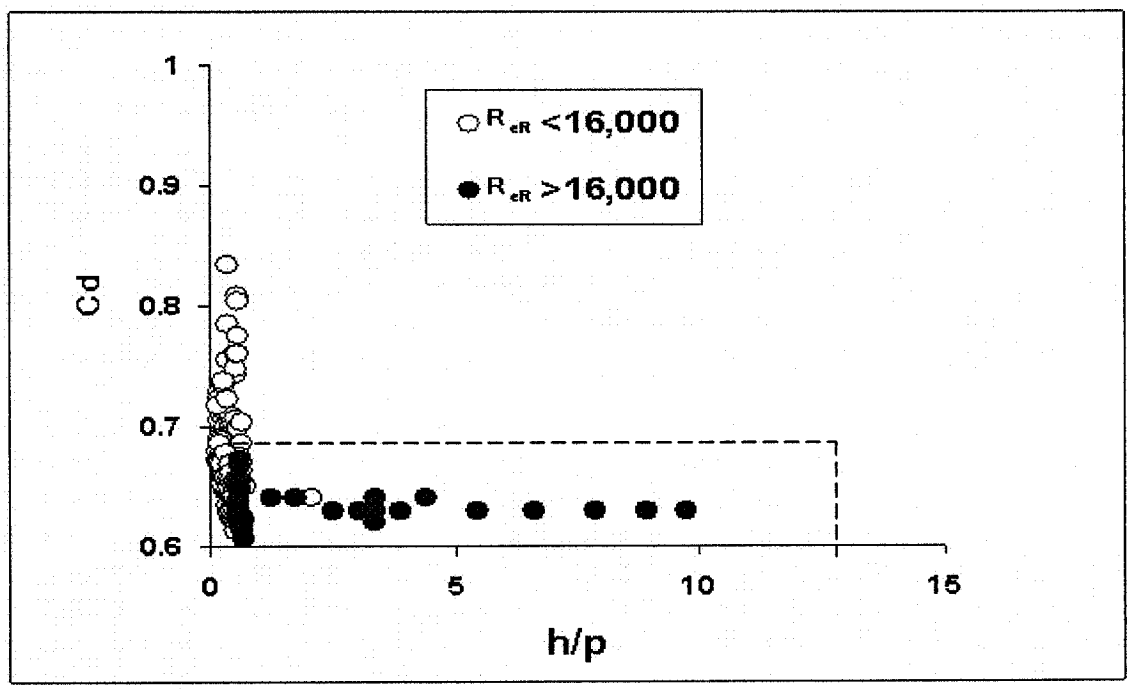

Fig. 4.1 Cd Vs h/p for Rectangular and V-shaped Multi-slit Weirs

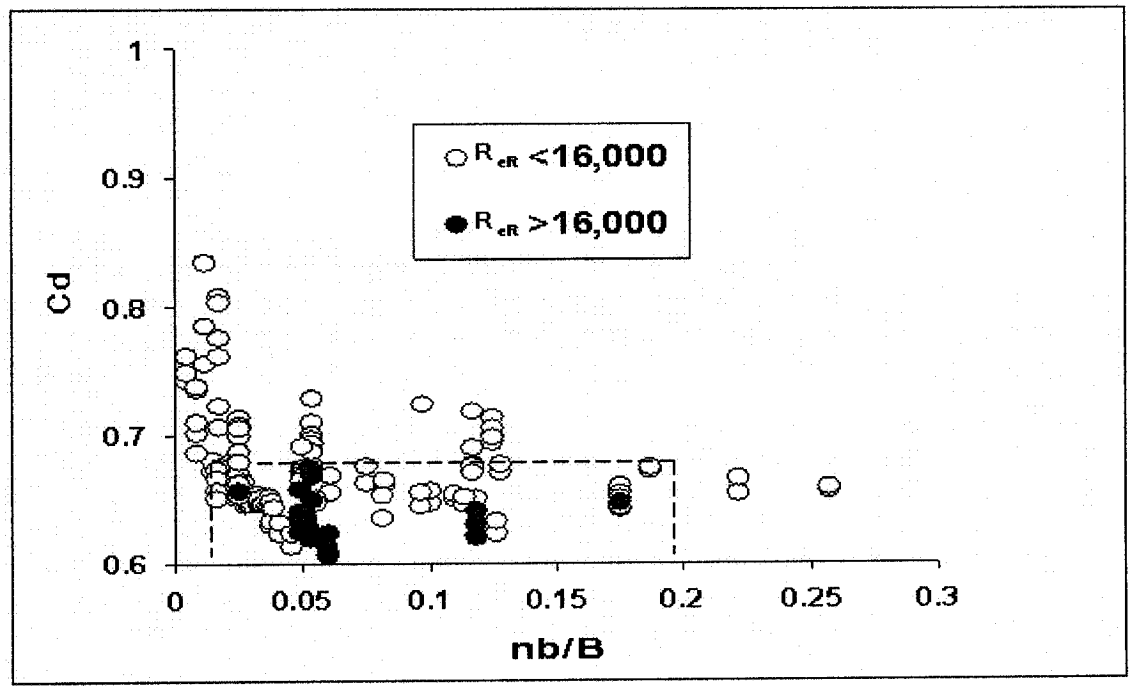

Fig. 4.2 Cd Vs nb/B for Rectangular and V-shaped Multi-slit Weirs

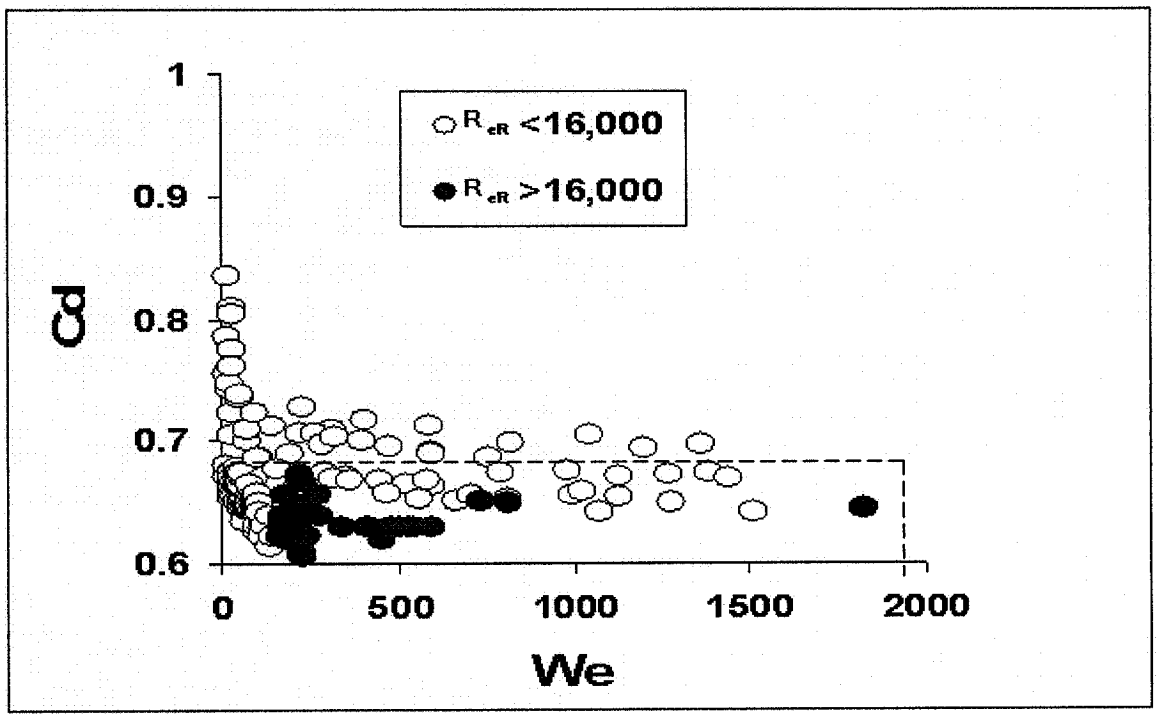

Fig. 4.3 Cd Vs We for Rectangular and V-shaped Multi-slit Weirs

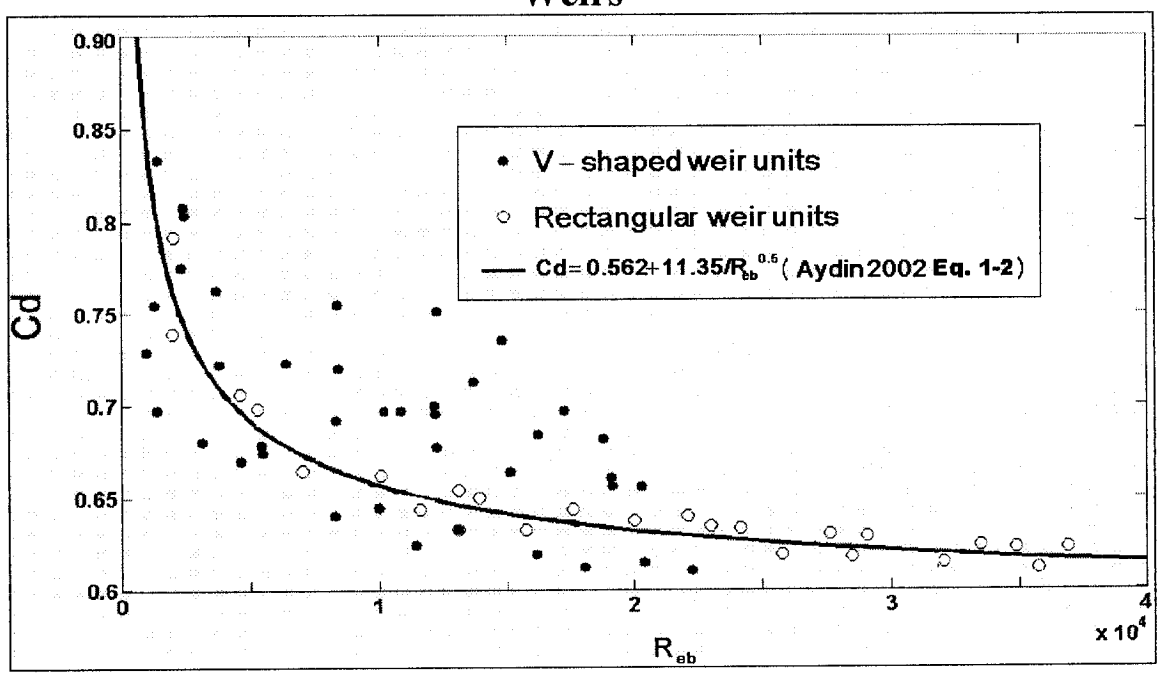

Fig. 4.4 Cd Vs R_{eb} for Rectangular and V-shaped Multi-slit Weirs

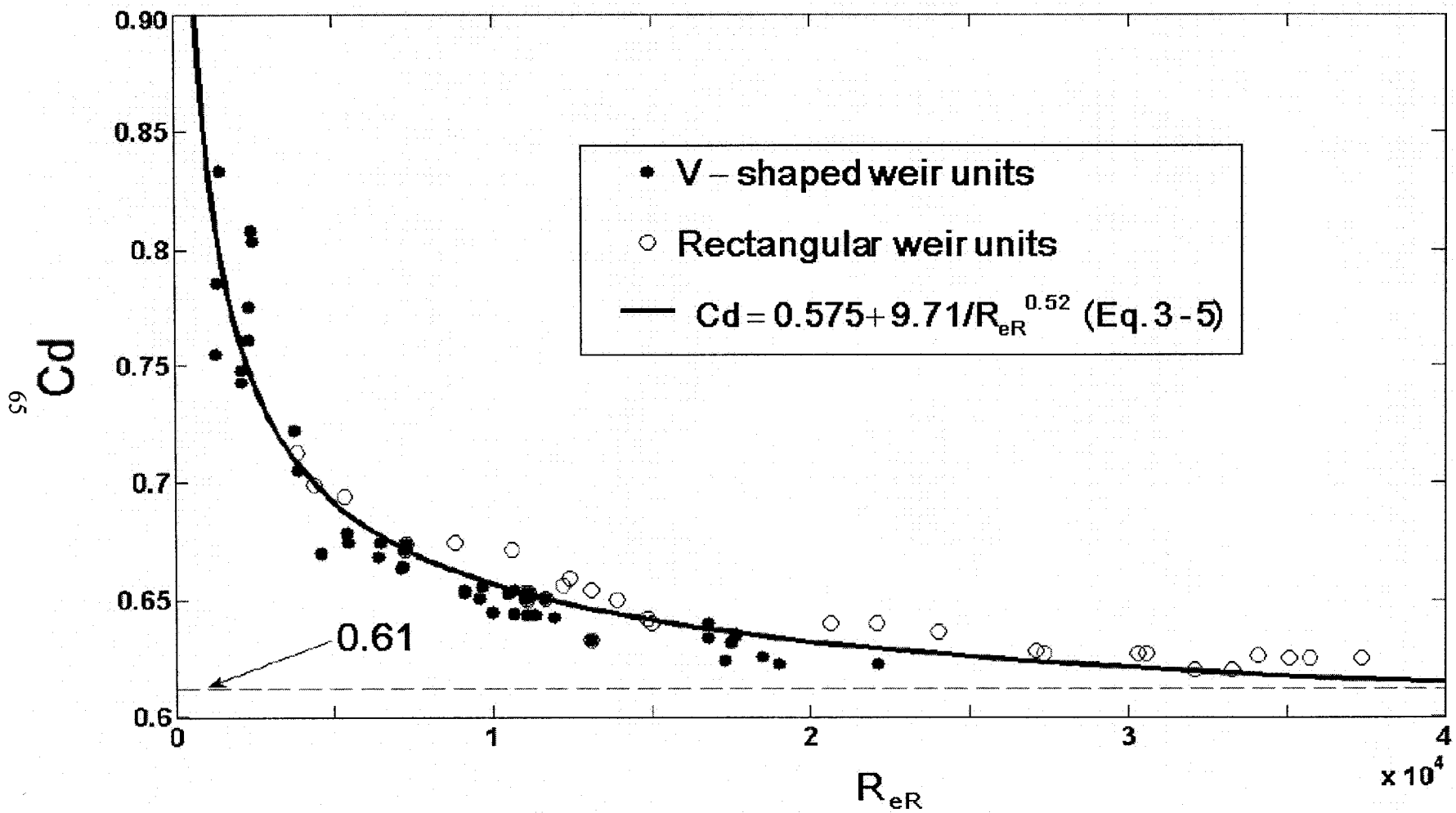

Fig. 4.5 Cd Vs R_{eR} for Rectangular and V-shaped Multi-slit Weirs

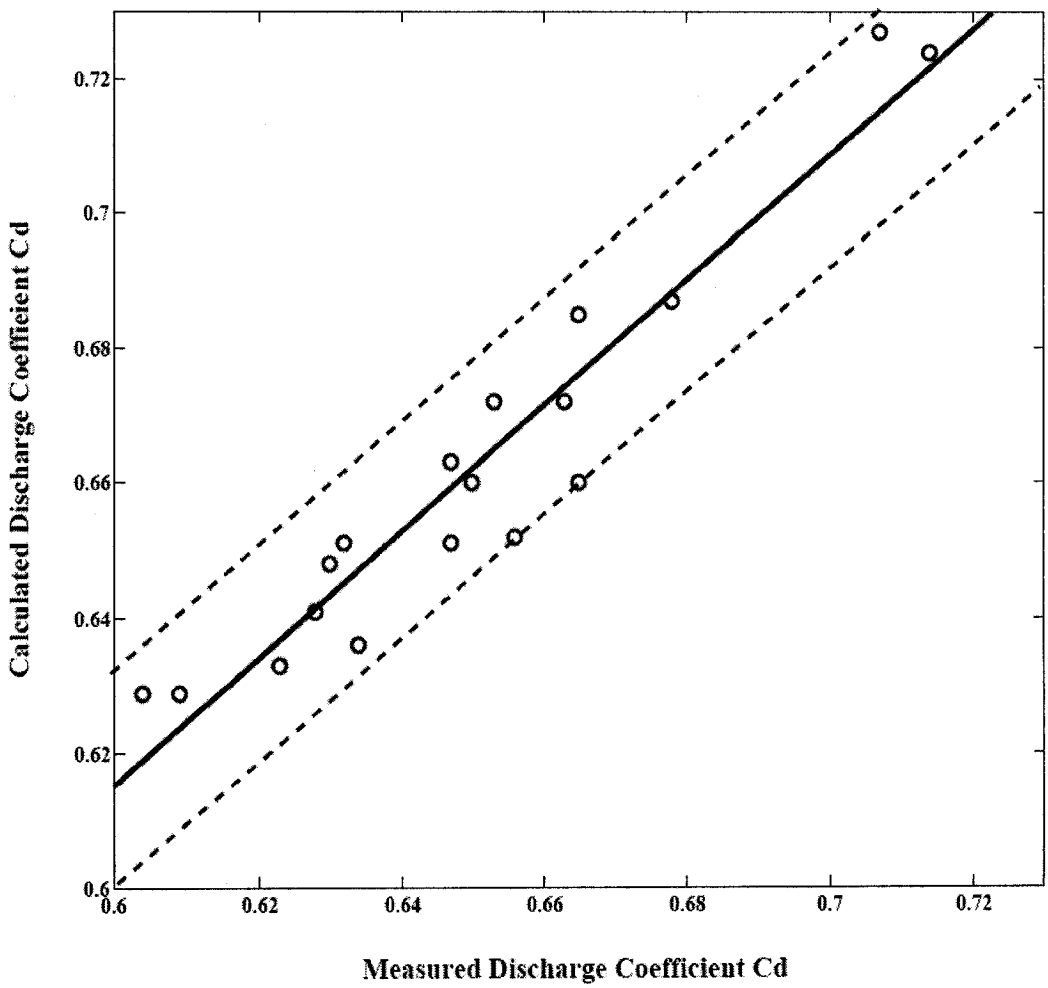

Fig.4.6 Comparison of Measured Cd Vs. Computed Cd in 95% Confidence Interval

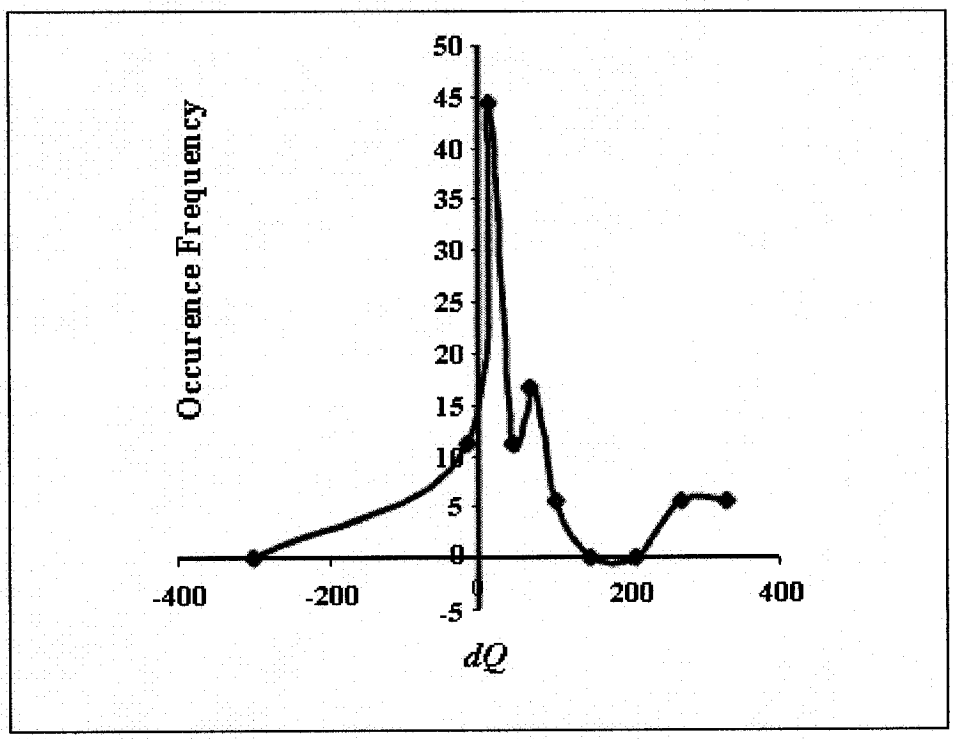

dQ	*F*
−300	0
−15	11.1
15	44.4
45	11.1
75	16.7
105	5.6
150	0
210	0
270	5.6
330	5.6

Fig. 4.7 Frequency Distribution of *dQ* (cm³/s)

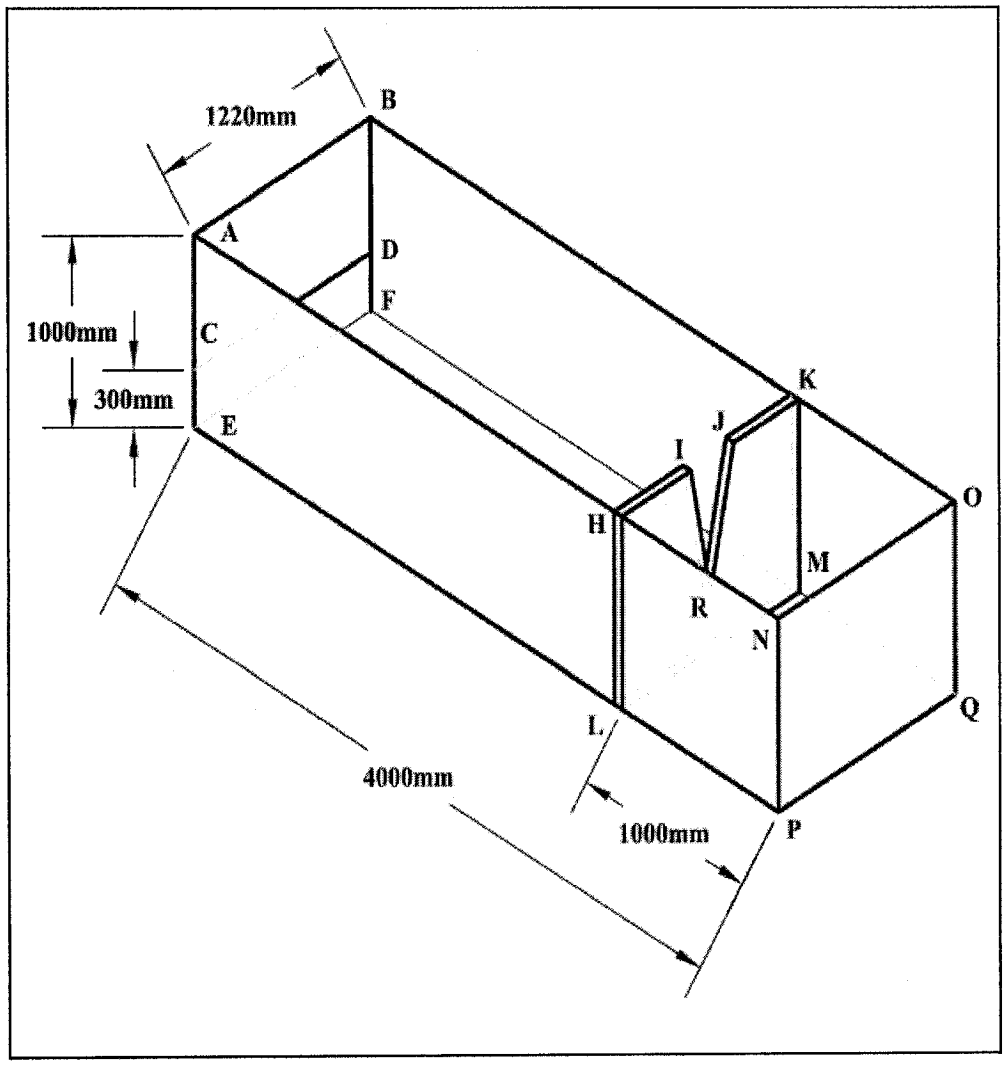

Fig.A.1 Computational Domain for V-shaped Weir

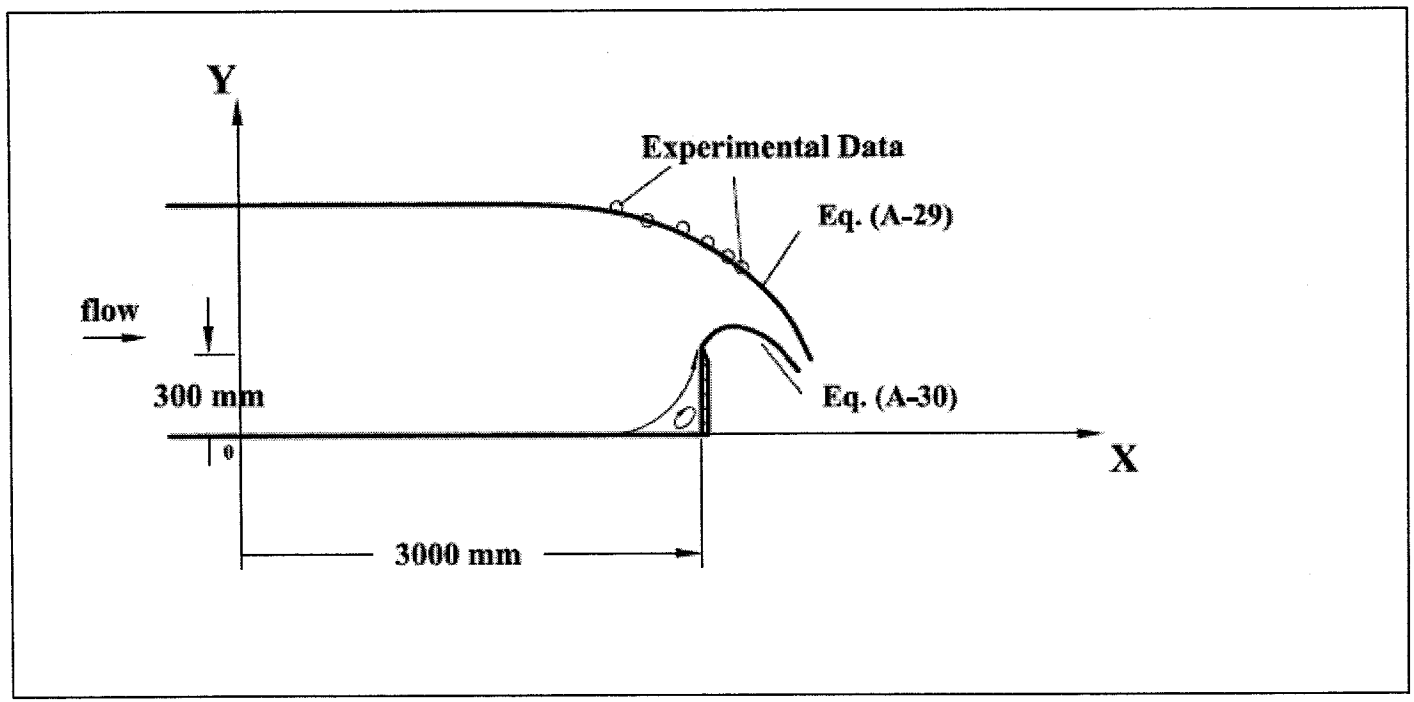

Fig. A.2 CFD Simulation of Water Surface Profile for V-shaped Weir

APPENDIX

THREE DIMENSIONAL SIMULATION OF FLOW OVER V-SHAPED WEIRS (OR NOTCHES)

This appendix introduces the 3D free surface turbulence model including boundary conditions and numerical algorithm. Also, in this appendix the simulation of flow past V-shaped (sharp-crested) weir in an open channel is presented very briefly. The predicted results are validated using selected test data. A good validated CFD code is helpful in predicting the flow characteristics of weir flow when the boundary conditions and flow configuration of weirs geometry are changed. Experimental procedures are generally expensive to conduct a variety of tests.

A.1 Computational Fluid Dynamics (CFD)

Computational Fluid Dynamics (CFD) has grown from a mathematical curiosity to become an essential tool in almost every branch of fluid dynamics. CFD is commonly accepted as referring to the broad topic encompassing the numerical solution, by computational methods of the governing equations, which describe fluid flow applying the Navier-Stokes equations, continuity and any additional conservation equations. As a developing science, it has received extensive attention throughout the scientific community since the advent of the personal computer.

There has been considerable growth in the development and application of CFD to all aspects of fluid dynamics. In the design and development, CFD programs are now

considered to be standard numerical tools, widely utilized within industry. As a consequence there is a considerable demand for specialists in the subject, to apply and develop CFD methods throughout engineering companies and research organizations.

Therefore, in recent years, a number of CFD commercial software packages have incorporated one or more models for calculating the free surface profile, while simultaneously solving the internal flow structure of (at least) the water phase by the usual methods. The two processes are interactive: the turbulence model, influential in developing the internal flow structure of the water phase, consequently affects the development of the free surface profile, the resistance and energy losses that it predicts; the free surface profile in effect defines the flow geometry of the water phase and thus the solution domain within which the turbulence model is applied.

A.2 RANS Model

Engineers are normally interested in knowing just a few quantitative properties of turbulent flow, such as the average forces on a body (and, perhaps, its distribution), the degree of mixing between two incoming streams of fluid, or the amount of a substance that has reacted.

For Reynolds-Average Navier-Stokes (RANS) equation, every variable can be written as:

$$\phi(x_i,t) = \bar{\phi}(x_i) + \phi'(x_i,t) \qquad \text{(A-1)}$$

For unsteady flows, the time dependent or unsteady Reynolds averaged Navier-Stokes (URANS) equations should be considered. Here the averaging time is greater than the

characteristics timescale of turbulence and smaller than the characteristics period for the time evolution of the mean properties (Deck et al 2002).

$$\overline{\phi}(x_i, t) = \lim_{n \to \infty} \frac{1}{N} \sum_{n=1}^{n} \phi(x_i, t) \tag{A-2}$$

Here, N is the number of members of the ensemble and must be large enough to eliminate the effects of the fluctuation. This type of averaging can be applied to any flow.

For unsteady flows, the time dependent or unsteady Reynolds averaged Navier-Stokes (URANS) equations should be considered. Here the averaging time is greater than the characteristics timescale of turbulence and smaller than the characteristics period for the time evolution of the mean properties (Deck et al 2002).

In the Reynolds-averaged approaches to turbulence, all the unsteadiness is averaged out assuming that the unsteadiness is regarded as part of turbulence. The Reynolds averaged Navier-Stokes equation (RANS) is shown,

$$\frac{\partial U_i}{\partial t} + U_j \frac{\partial U_i}{\partial x_j} = -\frac{\partial p}{\partial x_i} + \frac{\partial}{\partial x_j}(2\nu S_{ji} - \overline{u_j' u_i'}) \tag{A-3}$$

Here, p = pressure, t = time, U_i = velocity in x_i direction, the subscript i=1, 2, 3 and j=1, 2, 3.

Also, the continuity equation is:

$$\frac{\partial U_i}{\partial x_i} = 0 \tag{A-4}$$

The two-equation models are the most popular turbulence models in the numerical simulation of turbulent flows. The two-equation models are based on the Boussinesq

eddy-viscosity approximation, which assumes that the principal axes of the Reynolds stress tensor τ_{ij} are coincident with those of the mean strain-rate tensor s_{ij} at all of the points in a turbulent flow. The coefficient of proportionality between τ_{ij} and s_{ij} is the eddy viscosity ν_T. The specific Reynolds stress tensor based on the Boussinesq assumption is:

$$\tau_{ij} = -\overline{u_i' u_j'} = \nu_T S_{ij} - \frac{2}{3} k \delta_{ij} \tag{A-5}$$

In the two-equation models, both the k–ε model and the k-ω model are most widely used.

A. 2. 1 Wilcox (1998) k-ω model

Kinetic Eddy Viscosity:

$$\nu_T = k / \omega \tag{A-6}$$

Turbulence kinetic energy:

$$\frac{\partial k}{\partial t} + U_j \frac{\partial k}{\partial x_j} = \tau_{ij} \frac{\partial U_i}{\partial x_j} - \beta^* k\omega + \frac{\partial}{\partial x_j}\left[(\nu + \sigma^* \nu_T)\frac{\partial k}{\partial x_j}\right] \tag{A-7}$$

Specific dissipation rate:

$$\frac{\partial \omega}{\partial t} + U_j \frac{\partial \omega}{\partial x_j} = \alpha \frac{\omega}{k} \tau_{ij} \frac{\partial U_i}{\partial x_j} - \beta \omega^2 + \frac{\partial}{\partial x_j}\left[(\nu + \sigma \nu_T)\frac{\partial \omega}{\partial x_j}\right] \tag{A-8}$$

Closure coefficients and auxiliary relations:

$$\alpha = \frac{13}{15}, \qquad \beta = \beta_0 f_\beta, \qquad \beta^* = \beta_0^* f_{\beta^*}, \qquad \sigma = \frac{1}{2}, \qquad \sigma^* = \frac{1}{2} \tag{A-9}$$

$$\beta_0 = \frac{9}{125}, \qquad f_\beta = \frac{1 + 70 x_\omega}{1 + 80 x_\omega}, \qquad x_\omega = \left|\frac{\Omega_{ij}\Omega_{jk} S_{ki}}{(\beta_0^* \omega)^3}\right| \tag{A-10}$$

$$\beta_0^* = \frac{9}{100}, \quad f_{\beta^*} = \begin{cases} 1, & x_k \le 0 \\ \dfrac{1 + 680 x_k^2}{1 + 400 x_k^2}, & x_k > 0 \end{cases}, \quad x_k \equiv \frac{1}{\omega^3}\frac{\partial k}{\partial x_j}\frac{\partial \omega}{\partial x_j} \tag{A-11}$$

$$\varepsilon = \beta^* \omega k \qquad \text{and} \qquad l = k^{1/2} / \omega \tag{A-12}$$

$$\Omega_{ij} = \frac{1}{2}\left(\frac{\partial U_i}{\partial x_j} - \frac{\partial U_j}{\partial x_i}\right), \qquad S_{ij} = \frac{1}{2}\left(\frac{\partial U_i}{\partial x_j} + \frac{\partial U_j}{\partial x_i}\right) \tag{A-13}$$

A. 2. 2 Standard $k-\varepsilon$ model

Kinetic Eddy Viscosity:

$$\nu_T = C_\mu k^2 / \varepsilon \tag{A-14}$$

Turbulence kinetic energy:

$$\frac{\partial k}{\partial t} + U_j \frac{\partial k}{\partial x_j} = \tau_{ij} \frac{\partial U_i}{\partial x_j} - \varepsilon + \frac{\partial}{\partial x_j}\left[(\nu + \nu_T / \sigma_k)\frac{\partial k}{\partial x_j}\right] \tag{A-15}$$

Dissipation rate:

$$\frac{\partial \varepsilon}{\partial t} + U_j \frac{\partial \varepsilon}{\partial x_j} = C_{\varepsilon 1} \frac{\varepsilon}{k} \tau_{ij} \frac{\partial U_i}{\partial x_j} - C_{\varepsilon 1} \frac{\varepsilon^2}{k} + \frac{\partial}{\partial x_j}\left[(\nu + \nu_T / \sigma_\varepsilon)\frac{\partial \omega}{\partial x_j}\right] \tag{A-16}$$

Closure coefficients and auxiliary relations:

$$C_{\varepsilon 1} = 1.44, \quad C_{\varepsilon 2} = 1.92, \quad C_\mu = 0.09, \quad \sigma_k = 1.0, \quad \sigma_\varepsilon = 1.3 \tag{A-17}$$

$$\omega = \varepsilon / (C_\mu k) \quad \text{and} \quad l = C_\mu k^{3/2} / \varepsilon \tag{A-18}$$

A. 3 Boundary Conditions

A. 3. 1 Wall Functions

At the wall boundary, the wall-function approach proposed by Launder and Spalding (1974) is used for the two-equation turbulence modeling. The universal logarithmic law of the wall with smooth surfaces that is applicable to the fully turbulent region outside the

viscous sublayer is expressed as

$$\frac{u}{u_\tau} = \frac{1}{\kappa} \ln \frac{u_\tau y}{\nu} + C \qquad \text{A-19)}$$

Here, u = resultant velocity parallel to the wall at the first cell, u_τ = resultant friction velocity, $k = 0.41$, y = normal distance to the wall, ν = Kinematic viscosity and $C = 5.0$ for smooth surfaces. For rough surfaces, one has to consider the effects of roughness of the wall surface and the constant C should be changed. For fully rough wall, Eq. (A-19) must be considered,

$$\frac{u}{u_\tau} = \frac{1}{\kappa} \ln \frac{y}{k_s} + 8.5 \qquad \text{(A-20)}$$

Here, k_s denotes the average height of surface roughness.

While dealing with the $k-\omega$ model, one should consider (Wilcox 1994 and 2000, Neary et al. 1999).

$$\omega = S_R \frac{u_\tau^2}{\nu} \qquad \text{(A-21)}$$

Here,

$$S_R = \begin{cases} \left(\frac{50}{k_s^+}\right), & k_s^+ < 25 \\ \left(\frac{100}{k_s^+}\right), & k_s^+ \geq 25 \end{cases}$$

and $k_s^+ = \frac{u_\tau k_s}{\nu}$

The near wall values of turbulent kinetic energy k and the specific dissipation rate are specified assuming local equilibrium of turbulence (Wilcox 2000):

$$k = \frac{u_\tau^{\,2}}{\sqrt{\beta_o^*}}, \quad \omega = \frac{u_\tau}{\sqrt{\beta_o^*}\kappa y}, \varepsilon = \left(\beta_o^*\right)^{3/4} \frac{k^{3/2}}{\kappa y} \quad \text{here, } \beta_0^* = \frac{9}{100} \text{ (A-21)}$$

It is noted that during the numerical simulation the grid cells next to the wall boundary are constructed well within the turbulent region $30 < y^+ \equiv \frac{u_\tau y}{\nu} < 130$ (Rameshwaran and Naden 2003).

A. 3. 2 Free Surface Boundaries

For numerical simulations related to open channel flows, the free surface condition should be considered. The free surface elevation can be assumed horizontal if the water surface deformation is not large. This is the solid lid approximation. In most cases, it is necessary to know the shape of the free surface. Many methods have been used to find the shape of a free surface. They can be simply classified into two major groups (Ferziger and Peric, 2002).

Interface-Tracking Scheme

This method defines the free surface as a sharp interface. The motion of the free surface has to be traced in the computation. Boundary-fitted grids are used, and they are readjusted each time the free surface is moved. In order to get trace of a sharp interface, very small time steps and grids should be used.

At the free surface, the boundary for the vertical velocity, however, is determined by satisfying the free-surface kinematics condition (in Cartesian coordinates), i.e,

$$u_z = \frac{\partial H}{\partial t} + u_x \frac{\partial H}{\partial x} + u_y \frac{\partial H}{\partial y} \qquad \text{(A-22)}$$

Here, u_x, u_y, and u_z denote flow velocity in x-direction, y-direction, and z-direction, respectively. H denotes the water depth, and t denotes time.

The pressure variable p is defined as a deviation from the hydraulic pressure, that is,

$$p = p_0 + gH \tag{A-23}$$

Here, p_0 denotes the pressure of free surface, and g denotes the specific gravity. This scheme is applied in the numerical simulation of some flow cases (Meselhe and Sotiropoulos 2000, Huang et al. 2002).

Interface-Capturing Scheme

This interface-capturing method does not define a sharp boundary. The computation is performed on a fixed grid. The motions of the water surface are limited in the grid geometry. The shape of the free surface is determined by cells that are partially filled.

The interface-capture method is easier than the interface-tracking method for computation. One need not change the grid during the simulation, which saves lots of times. The typical scheme in the interface-capture method is the volume of fluid (VOF) scheme. This scheme is used by many researchers (Mohapatra et al. 2001, Chen et al. 2002 and Maronnier et al. 2003). Here, the VOF scheme is introduced.

For the VOF scheme, one has to introduce a new variable c, which is called the void fraction. The void fraction c is defined by the quantity ratio of water to air in a cell. Generally, c = 1 when the cell is filled fully by water and c = 0 when the cell is filled fully by air. The governing equation of c is follow (Ferziger and Peric 2002):

$$\frac{\partial c}{\partial t} + \frac{\partial (U_i c)}{\partial x_i} = 0 \qquad \text{(A-24)}$$

Also c must satisfy the condition

$$0 \leq c \leq 1 \qquad \text{(A-25)}$$

Therefore, for free surface problems, one has to solve the equation for the void fraction besides the conservation equation for mass and momentum.

Alternatively, near the free surface boundary, one can treat both fluids as a single fluid, whose properties vary in space according to the volume fraction of each phase, i.e.:

$$\phi = \phi_1 c + \phi_2 (1 - c) \qquad \text{(A-26)}$$

Here, ϕ = density, molecular viscosity and turbulence quantities. Subscripts 1 and 2 denote the two fluids (e.g. water and air).

For the velocity components near the free surface boundary, it is assumed that the velocity of air is equal to the velocity of water. Far from the free surface boundary, the velocity is equal to zero in the air. The pressure near the free surface boundary is obtained using linear extrapolation method from the interior of the water domain.

A. 3. 3 Inlet Boundaries

At the inflow boundary, the zero derivative condition is applied to velocity components and turbulence parameters. In some cases, at inflow boundary, the uniform flow condition for flow velocities and turbulence quantities is used simply. The pressure at the inlet boundary is linearly extrapolated from the interior of the domain. The water surface level can be specified or obtained using the linear extrapolation method.

A. 3. 4 Outlet Boundaries

The pressure is prescribed, and is usually set to zero. The flow related data for flow velocities and turbulence quantities are obtained by using the linear extrapolation of computed values in the two adjacent interior points that are just above the exit plane. This boundary condition is also termed as the zero diffusion flux condition.

At the outlet boundary for open channel, the water surface level can be specified or obtained using the linear extrapolation method.

A. 4 Numerical Algorithm

A. 4. 1 Finite Volume Methods

Finite Volume Method (FVM) is usually used in computational fluid dynamics. The integral forms of those governing equations as mentioned earlier are transformed onto the computational domain and they are then discretized with the finite-volume method. The computational domain is subdivided into a finite number of small Control Volumes (CVs) by grids. The computational node is usually assigned to the CV center. The integral forms of those governing equations apply to each CV, as well as to the solution domain as a whole. If one sums equations for all CVs, one can obtain the global conservation equation, since the surface integral over inner CV faces cancel out. To obtain an algebraic equation for each CV, the surface and volume integrals need be approximated.

A. 4. 2. Discretization of the Convective Terms

Numerous forms of interpolation are available. Some are less efficient and some are less

stable in the course of iteration. It is very important to choose a right interpolation scheme. Usually, first order or second order schemes are used. Higher-order schemes, such as QUICK (Quadratic Upwind Interpolation for Convective Kinematics) and second-order upwind schemes, are possible options for high precision requirements. The Upwind Difference Scheme (UDS) is the only approximation that unconditionally satisfies the boundedness criterion (Ferziger and Peric 2002). It is however a first order scheme, numerically diffusive, and requires very fine grids to obtain accurate solutions. The central difference scheme (CDS) is a second order scheme. It is more accurate, but it may produce oscillatory solutions and the convergence rate is usually slower (Ferziger and Peric 2002). The Deferred Correction Scheme (DCS) combines the advantages of both UDS and CDS. DCS utilizes the UDS in implicit method, and the difference between UDS and CDS is calculated explicitly using values from the previous iteration.

$$F_e = F_e^{UDS} + (F_e^{CDS} - F_e^{UDS})^{old} \quad \text{(A-27)}$$

Here, F represents the convective term. DCS was also mentioned by Huang (2000).

A. 4. 3 Grid Generation

For a regular geometry, it is simple to choose the grid. The grid lines follow the coordinate directions. However, most flows in engineering practice involve complex geometries, which cannot be readily fitted with Cartesian grids. In order to apply such a simple grid to solution domains with inclined or curved boundaries, the boundaries have to be approximated to staircase-like steps. If this approach is used, it results in errors in the solution. Boundary-fitted-orthogonal grids and curvilinear coordinates are most often used to calculate flows in complex geometries (most commercial codes use such grids).

They can be structured, block-structured, or unstructured. The advantage of such grids is that they can be adapted to any geometry. Since the grid lines follow the boundaries, the boundary conditions are easier to implement than with the stepwise approximation of the curved boundaries.

In this study, built a domain as the experimental size, and separate it the 16 blocks, each block is meshed with different size, which generates a fine mesh in the vicinity of the boundary or in the flow region where the flow changes rapidly. Grids near the wall boundary have to satisfy the requirement of the wall function.

A. 5 Solutions Procedures

The solutions procedures are summarized as following:

1) Generate grid

As mentioned above, generati a 4000 mm long, 1220mm wide and 1000mm height domain, (Fig. A.1) which has 16 blocks, each block has its mesh size and mesh ratio. The total number of cell is 333,278. The exact information of the cell shows on the Table (5.5)

2) Set flow parameters and choose models

In present study, the RANS equations are applied to solve the free overfall problem in a rectangular open channel. The three-dimension (3D) standard two-equation k–ε turbulence model is adopted for the numerical simulation. The fractional Volume of Fluid (VOF) method is an efficient method for treating the complicated free-surface problem. The pressure-velocity coupling is achieved using the PISO algorithm (Issa, 1986). The time step is 0.005 second.

The results of simulation are validated using the experimental data pertaining to surface profiles. The predicted surface profiles also agree well with the theoretical results and the simulated results. The upper surface of the nappe is displayed as:

$$-y = 1.50x^2 - 8.4x + 11.0 \tag{A-29}$$

and the nether water surface of nappe is:

$$-y = 3.0x^2 - 18.6x + 28.6 \tag{A-30}$$

3) Set boundary conditions and initial conditions

At the wall boundary, the standard wall-function is used, and the V-notch is defined as a wall IHLMKJR (Fig. A.1). At the inlet CDFE (Fig. A.1), known flow velocities and turbulent quantities are prescribed. Here, the uniform flow condition for the horizontal velocity is provided. The outlet LMQP and NOQP downstream from the end depth (Fig. 5.1) are defined as pressure boundaries. This allows the water to flow out freely. All the air boundaries are defined as pressure boundaries with zero pressure. For the free surface boundary, the VOF model is used.